https://ntrs.nasa.gov/search.jsp?R=19700026372 2020-02-14T18:58:11+00:00Z

N70-35600

NASA CONTRACTOR
REPORT

NASA CR-61332

ANALYSIS OF EXHAUST PLUMES FROM SKYLAB-CONFIGURATION R-4D ATTITUDE CONTROL MOTORS

By A. W. Ratliff, B. J. Audeh, and D. D. Thornhill

Lockheed Missiles and Space Company
Huntsville Research and Engineering Center
Huntsville Research Park, 4800 Bradford Dr.
Huntsville, Alabama

OCT 1970
RECEIVED
NASA STI FACILITY
INPUT BRANCH

March 1970

CASE FILE
COPY

Prepared for

NASA-GEORGE C. MARSHALL SPACE FLIGHT CENTER
Marshall Space Flight Center, Alabama 35812

1. Report No.	2. Government Accession No.	3. Recipient's Catalog No.
CR-61332		

4. Title and Subtitle	5. Report Date
ANALYSIS OF EXHAUST PLUMES FROM SKYLAB-CONFIGURATION R-4D ATTITUDE CONTROL MOTORS	March 1970
	6. Performing Organization Code
7. Author(s) A. W. Ratliff, B. J. Audeh, D. D. Thornhill	8. Performing Organization Report No. HREC/20082-22 LMSC/HREC D162171
	10. Work Unit No.
9. Performing Organization Name and Address Lockheed Missiles & Space Company Huntsville Research & Engineering Center Huntsville Research Park, 4800 Bradford Drive Huntsville, Alabama	11. Contract or Grant No. NAS8-20082
	13. Type of Report and Period Covered Contractor Report
12. Sponsoring Agency Name and Address NASA-Marshall Space Flight Center Marshall Space Flight Center, Alabama, 35812	14. Sponsoring Agency Code

15. Supplementary Notes

16. Abstract

The exhaust plume flow field of the Skylab (formerly AAP) configuration reaction control system (RCS) engines has been determined analytically as a preliminary step in the prediction of heating rates, forces, and contamination effects due to these plumes. The engine used, designated R-4D, burns nitrogen tetroxide and monomethylhydrazine (N_2O_4/MMH) propellant. Engine configurations, nozzle geometries, propellant description, and operating conditions were supplied by MSFC, Huntsville, Alabama; the Marquardt Corp., Van Nuys, California; and MSC, Houston, Texas. Plume flow fields in a vacuum environment were calculated for the engine used on the Command Service Module. Calculations began in the combustion chamber, extended through the nozzle, and continued into the plume to about 50 feet axially and radially from the engine. Flow striations (oxidizer-to-fuel variations) were considered in the analysis based on injector information supplied by MSC. A thermochemical program was used to define combustion product species concentrations and thermodynamic properties of the propellant system. A one-dimensional streamtube solution was used to define the physical and thermodynamic properties after equilibrium combustion. An equilibrium chemistry ducted mixing analysis was made through the combustion chamber. A time-dependent transonic solution was used to describe the two-dimensionality of the flow in the convergent section of the nozzle and through the nozzle throat. A method-of-characteristics solution was begun at the nozzle throat using equilibrium thermochemical properties up to a point in the flow at which a kinetic analysis indicated that the flow was chemically frozen. The plume was then generated using the nozzle exit conditions as starting information. The nozzle boundary layer effect on the plume was included and the region where non-continuum conditions may exist is indicated. Two shock waves were considered and treated in this analysis. The nozzle shock and its reflection from the nozzle axis were computed as integral parts of the total flow field. Also included in this analysis is a correlation study of several R-4D engine and plume parameters. This information provides justification for the particular oxygen-to-fuel gradient used as well as verification of the general analysis procedure.

17. Key Words (Suggested by Author(s))	18. Distribution Statement
	PUBLIC RELEASE E. D. Geissler E. D. GEISSLER, Dir, Aero-Astrodynamics Lab, MSFC

19. Security Classif. (of this report)	20. Security Classif. (of this page)	21. No. of Pages	22. Price*
Unclassified	U	57	

*For sale by the Clearinghouse for Federal Scientific and Technical Information Springfield, Virginia 22151

FOREWORD

This report presents the results of work performed by Lockheed's Huntsville Research & Engineering Center while under subcontract to Northrop Nortronics (NSL PO 5-09287) for the Aero-Astrodynamics Laboratory of Marshall Space Flight Center (MSFC), Contract NAS8-20082. This task was conducted in response to the requirement of Appendix B-1, Schedule Order No. 147 under the technical cognizance of Homer B. Wilson, Jr., Terry F. Greenwood and David C. Seymour.

ACKNOWLEDGMENT

The authors wish to acknowledge the contribution of Joseph L. Sims of the Fluid Mechanics Research Office of the Aero-Astrodynamics Laboratory (MSFC), for helpful consultations during portions of this study.

SUMMARY

The exhaust plume flow field of the Skylab (formerly AAP) configuration reaction control system (RCS) engines has been determined analytically as a preliminary step in the prediction of heating rates, forces and contamination effects due to these plumes. The engine utilized, which is designated R-4D, burns nitrogen tetroxide and monomethlyhydrazine (N_2O_4/MMH) propellant.

Engine configurations, nozzle geometries, propellant description, and operating conditions were supplied by three agencies: (1) NASA-Marshall Space Flight Center, Huntsville, Alabama; (2) the Marquardt Corporation, Van Nuys, California; and (3) NASA-Manned Spacecraft Center, Houston, Texas.

Plume flow fields in a vacuum environment were calculated for the engine used on the Command Service Module. Calculations began in the combustion chamber extended through the nozzle and continued into the plume to about 50 feet axially and radially from the engine.

Flow striations (oxidizer-to-fuel variations) were considered in the analysis based on injector information supplied by the Manned Spacecraft Center. A thermochemical program was used to define combustion product specie concentrations and thermodynamic properties of the propellant system. A one-dimensional streamtube solution was used to define the physical and thermodynamic properties after equilibrium combustion. An equilibrium chemistry ducted mixing analysis was made through the combustion chamber. A time-dependent transonic solution was used to describe the two dimensionality of the flow in the convergent section of the nozzle and through the nozzle throat. A method-of-characteristics solution was begun at the nozzle throat using equilibrium thermochemical properties up to a point in the flow at which a kinetic analysis indicated that the flow was chemically frozen. The plume was then generated using the nozzle exit conditions as starting information. The nozzle

boundary layer effect on the plume was included and the region where non-continuum conditions may exist is indicated.

Two shock waves were considered and treated in this analysis. The nozzle shock and its reflection from the nozzle axis were computed as integral parts of the total flow field. Also included in this analysis is a correlation study of several R-4D engine and plume parameters. This information provides justification for the particular oxygen-to-fuel gradient used as well as verification of the general analysis procedure.

CONTENTS

Section		Page
	FOREWORD	ii
	SUMMARY	iv
1	INTRODUCTION	1
2	METHOD OF ANALYSIS	3
	2.1 Combustion Chamber and Nozzle Throat	3
	2.2 Nozzle Expansion	4
	2.3 Nozzle Shock Waves	4
	2.4 Plume Analysis	5
3	DISCUSSION	9
	3.1 Combustion Analysis	10
	3.2 Transonic Analysis	12
	3.3 Nozzle Freezing Points	16
	3.4 Nozzle and Plume Calculation	22
4	PRESENTATION OF RESULTS	24
	4.1 Discussion of Results	24
	4.2 Summary of Results	37
	REFERENCES	39
	APPENDIX A: Supplementary Study of the R-4D Engine Using N_2O_4/A-50 Propellants	A-1

LIST OF ILLUSTRATIONS

Table		Page
1	Nominal R-4D Engine Operating Characteristics for Command Service Module Reaction Control System Application	15
2	Thermodynamic Properties of an Equilibrium/Frozen Monomethylhydrazine/Nitrogen Tetroxide System for the Oxidizer-to-Fuel Mass Ratio Range of the R-4D Engine	21
3	Plume Starting Line Properties	23
4	Constituent Mole Fractions at the Freezing Point Pressures for the R-4D Engine Nozzle Flow with an O/F Variation from 1.24 to 3.07 with an N_2O_4 Propellant System	38

Figure		
1	Sketch of the R-4D Rocket Engine	11
2	Properties at the End of the Preigniter and at the Inlet to the Convergent Section of the Nozzle (1.276 inches from the end of the Preigniter)	13
3	Nozzle Contour for R-4D Engine Used in the Lunar Excursion Module and Command Service Module Reaction Control Systems	14
4	Starting Line Conditions for MOC Calculation. Starting Line at 0.124 in. from Throat	17
5a	Constituent Mole Fraction Variation Along the Centerline of the R-4D Engine Nozzle at an O/F of 3.07 for an MMH/N_2O_4 Propellant System	18
5b	Constituent Mole Fraction Variation Along the Centerline of the R-4D Engine Nozzle at an O/F of 3.07 for an MMH/N_2O_4 Propellant System	19
5c	Constituent Mole Fraction Variation Along the Centerline of the R-4D Engine Nozzle at an O/F of 3.07 for an MMH/N_2O_4 Propellant System	20
6	Location of Streamlines and Mass Flow Distribution (Percent of Total) in R-4D Plume Flowfield	25
7	Lines of Constant Mach Number in R-4D Plume Flowfield	26
8	Lines of Constant Temperature (^{o}R) in R-4D Plume Flowfield	27

LIST OF ILLUSTRATIONS (Continued)

Figure		Page
9	Lines of Constant Static Pressure (psfa) in R-4D Plume Flowfield	28
10	Lines of Constant Density (slugs/ft^3) in R-4D Plume Flowfield	29
11	Lines of Constant Flow Angle (degrees) in R-4D Plume Flowfield	30
12	Lines of Constant Pitot Pressure (psfa) in the R-4D Plume Flowfield	31
13	Lines of Constant O/F Ratio in R-4D Plume Flowfield	32
14	Mach Number and Temperature Distribution Along Centerline of R-4D Plume Flowfield	33
15	Pitot and Static Pressure Distribution Along Centerline of R-4D Plume Flowfield	34
16	Density Distribution Along Centerline of R-4D Plume Flowfield	35
17	Velocity Distribution Along Centerline of R-4D Plume Flowfield	36
A-1	Comparison of Measured and Calculated Pitot Pressures One-Half Inch Downstream of Exit Plane	A-3
A-2	Comparison of Measured and Calculated Pitot Pressures Three and One-Half Inches Downstream of Exit Plane	A-4
A-3	Comparison of Measured and Calculated Pitot Pressures Six and One-Half Inches Downstream of Exit Plane	A-5
A-4	Radial Heating Rate Variation 2.5 Inches from Exit Plane	A-6

Section 1
INTRODUCTION

When attitude control maneuvers are required for the Skylab configuration, small reaction motors are employed to effect these maneuvers. Two separate reaction control systems are utilized in the Skylab configuration: (1) the Auxiliary Propulsion System (APS) which is located on the aft end of the S-IVB Orbital Workshop; (2) a reaction control system (RCS) on the Command Service Module (CSM). When some of the motors of these systems are operated, various parts of the overall configuration may be subjected to direct or indirect impingement of the exhaust plume from the operating engine. An analysis of the Wet Workshop APS system engine is contained in Ref. 1. This report is concerned with the Marquardt R-4D engine used on the CSM.

The effects of plume impingement should be carefully assessed with respect to possible adverse forces and heating rates which may arise. The forces must be evaluated in order to determine system size and duty cycle as well as for structural loading effects. The heating rates due to impingement on various parts of the vehicle are also an important consideration. Some parts of the vehicle may have temperature-sensitive components for which the environment must be known in order to protect them properly. Another effect which must be evaluated is concerned with the possible contamination which may occur on the portions of the vehicle subject to plume impingement. It is important to be able to predict any changes which the vehicle surfaces may undergo due to the adverse rocket plume environment. Temperature control devices, for example, are dependent upon their surface optical properties for effective operation. Thus, if contamination changes these properties, the effective use of the device may be compromised.

In view of the many problems which arise due to plume impingement, it is important to predict adequately the resulting effect on a particular vehicle or portion of a vehicle. In order to make predictions of plume impingement

effects; an accurate and detailed description of the plume must be available. It is the purpose of the study reported herein to provide the analytical description of plumes from the Skylab configuration Reaction Control System motors (R-4D) so that their effects on the vehicle can be analyzed. The data presented in this report are for free plumes exhausting into a vacuum environment and do not include the impingement effects per se, but provide basic information necessary for conducting impingement analyses.

Section 2
METHOD OF ANALYSIS

The importance of plume impingement with respect to the Skylab configuration dictates that the plume data utilized be as detailed as possible. Since there are numerous methods for analyzing plumes based upon various assumptions, the methodology used in this study is discussed in some detail.

2.1 COMBUSTION CHAMBER AND NOZZLE THROAT

The calculational procedure was begun with a combustion chamber analysis consisting of a streamtube combustion solution (Ref. 2) coupled with an equilibrium, ducted, mixing calculation (Ref. 3). Because radial mixture ratio gradients were present, variations in the combustion gas properties were accounted for by using a number of streamtubes each with a different mixture ratio. The solution assumed the gases to be in chemical equilibrium. No radial pressure gradients were allowed, and the inlet conditions at the injector face were determined by the extensive correlation study discussed in the Appendix.

The Streamtube program (Ref. 2) was used to determine the physical and thermodynamic properties after equilibrium combustion to provide data for the ducted equilibrium mixing program (Ref. 3). The equilibrium mixing calculation was done for the flow through the combustion chamber, and the resultant properties at the entrance to the convergent section were used in the transonic solution. The transonic region of the R-4D engine was analyzed using a Lax-Wendroff-type of time-dependent solution. The two-dimensional effects are thus included in the transonic calculations. The program treats flows with oxidizer-to-fuel (O/F) gradients, and real gas equilibrium processes were used. The transonic program generated a starting line, i.e., initial conditions, for beginning a method-of-characteristics (MOC) calculation for the nozzle expansion section. The starting line derived in this fashion accounts

for combustion chamber momentum loss and radial flow striations, but does not account directly for combustion efficiency. Boundary layer and wall heat transfer in the combustion chamber were also neglected.

2.2 NOZZLE EXPANSION

Once the nozzle throat conditions were known, a MOC calculation was used to analyze the supersonic flow downstream of the throat. The Lockheed Method-of-Characteristics Computer Program (Ref. 4) was used to accomplish all the supersonic calculations for this study. The basic program of Ref. 4 was specially modified to handle the flow striations which existed in the engines. Initially, the flowfield chemistry was assumed to be in equilibrium and the gas properties were obtained from the NASA-Lewis Research Center Thermochemical program (Ref. 5). To determine the chemical reaction freeze point, the pressure distribution along the nozzle wall and centerline obtained from the chemical equilibrium solution were used as boundary conditions for a one-dimensional calculation using finite rate chemistry (Ref. 6). The streamlines analyzed in each case consisted of the nozzle centerline and the wall contour. When the "freeze" points were determined from the finite-rate analysis, the thermochemistry data were regenerated using the pressure freeze option of the NASA-Lewis program (Ref. 7). This option allows the thermochemical calculations to switch from equilibrium to frozen at a specified pressure which was obtained from the kinetics analysis of Ref. 6. The equilibrium/frozen gas properties were then used in a second calculation of the nozzle flow field which approximately accounted for the finite-rate effects on the resulting flow field. Because mixture ratio gradients were present, each streamline was analyzed at its own local O/F value and the "freeze points" on streamlines between the centerline and nozzle wall were assumed to vary linearly with O/F ratio.

2.3 NOZZLE SHOCK WAVES

Most contoured nozzles give rise to the formation of an internal shock wave. The shock is initiated by a discontinuity in the second derivative of the contoured nozzle at the junction between the expansion section, near the nozzle

throat, and the recurved section which comprises the remainder of the nozzle. This shock is generally weak at its origin and gradually increases in strength, becoming quite strong as it intersects the nozzle axis of symmetry. A detailed description of the plume requires that the effect of this shock on the local flow properties be taken into account. Thus in keeping with the study objective, this shock wave was computed as an integral part of the nozzle flowfield analysis.

When shock waves, in general, approach the nozzle axis of symmetry, two things may happen. First, if the shock is strong enough, a Mach disk may form which causes the flow to "shock down" into the subsonic regime. Weaker shocks, however, may go through a regular reflection, at least in an inviscid analysis, such that the flow remains supersonic even behind the reflected leg of the shock system. Shock waves encountered in the nozzles of this study were weak and reflected regularly at the axis.

2.4 PLUME ANALYSIS

When the nozzle solution was completed, including the incident nozzle shock, the analysis was continued into the plume flow field. The initial conditions, i.e., start line, for the plume analysis consisted of the downstream shock points from the nozzle analysis. However, because the shock itself does not progress all the way to the nozzle wall, other points from the nozzle analysis were also required. These points consisted of flowfield data points proceeding from the shock wave, across the nozzle exit plane, to the nozzle lip. The flowfield chemistry used by the plume analysis was the same as that used for the nozzle. This was possible because the kinetics analysis had indicated that the flowfield chemistry was frozen inside the nozzle and, since the flow continually expands into the plume, the chemistry should then, remain frozen.

When the procedure was restarted to generate the plume, the incident nozzle shock was reflected from the nozzle axis and continued throughout the plume. The plume was allowed to expand to a vacuum environment as a boundary condition. This is, of course, quite impractical in a numerical solution,

because of the extremely high Mach numbers and pressures which approach zero. To circumvent the numerical problems, the expansion was only allowed to approach the limiting expansion angle within 10 deg and the solution was stopped at that point.

2.4.1 Non-Continuum Effects

When a plume expands into a vacuum, its density eventually becomes so low that the flow no longer obeys continuum gas dynamics laws. Ideally, plume calculations should consider non-continuum effects (Ref. 8). Continuum analyses, for instance, should be stopped when the flowfield parameters and gradients satisfy the Knudsen number criteria for free molecular flow, i.e., vibrational, rotational and translational energy modes "frozen". The calculations should then be continued along streamlines from an apparent source, assuming that the streamlines remain straight and the molecular velocities are all in the direction of the flow. In the free molecular regime, therefore, the stream velocity is constant and the density varies in inverse proportion to the cross-sectional area of the stream tube. For the analysis reported here, continuum gas dynamic relations were employed throughout the flow. Except for deviation of the translational temperature, as the flow approaches free molecular conditions, the continuum analysis is a good approximation. A physical explanation of this phenomenon is that in using the method-of-characteristics continuum analysis the angle between the streamlines and the Mach lines becomes very small, such that there is little lateral interaction between streamlines, thus approximating free-molecule flow. A calculation was performed, however, of the location of the translational "freezing" line to indicate incipient free-molecule flow.

2.4.2 Nozzle Wall Boundary Layer

Several recent studies have indicated that the presence of a nozzle wall boundary layer can have a significant effect on the local exhaust plume properties. Boynton in Ref. 9 discusses the inviscid expansion of nozzle boundary

layers from various engines ranging in thrust from 10 lb to 80,000 lb. His calculations indicate deviations which increase with expansion angle. Above 75 degrees expansion angle, for instance, differences in dynamic pressure of a factor of 10 were found.

Another nozzle wall boundary layer investigation was carried out in Ref. 10. A typical small RCS engine was analyzed with and without the boundary layer. Every input parameter, as well as the characteristic mesh size, was identical so that the boundary layer effect was the only difference between the two cases. As in Ref. 9, this study shows significant variations in the plume due to the boundary layer, especially in the outer 50% of the flow.

In light of these studies, the nozzle wall boundary layer was included in the present study, and its effect is inherent in the results presented in this report.

2.4.3 Condensation

The condensed form of the species present in the exhaust plume was not considered by the thermochemical or the flowfield analysis. Because of this, vapor pressure data for the various species were examined to determine if condensation could occur in the plume. Conditions in the continuum region which could lead to the formation of condensed H_2O were noted to exist for flows of Mach 10.0 and higher. Conditions favorable to the condensation of CO_2 exist for flows of Mach 15.0. Conditions favorable to the condensation of CO and N_2 exist for flows of Mach 29.0. Condensation will probably not occur for H_2. Solid particles may exist for the CO_2 and H_2O downstream of the region where conditions for the condensation are favorable. Due to the high velocities which exist in the plume flow field, condensed species may or may not be formed in the plume region shown. Incipient condensation and the calculation of a multi-phase plume flow field was not considered in this analysis.

2.4.4 Accuracy of the Predicted Plume Envionment

Determining a quantitative value for relating the accuracy of a rocket exhaust plume environment is a complex problem, involving numerous considerations. A detailed evaluation of plume environment accuracy is presented in Ref. 11 and can be used to estimate the gross accuracy of plume flow field parameters.

Section 3
DISCUSSION

For the R-4D engine analyzed, approximately 24 percent of the fuel is used for film cooling the engine and nozzle walls. Although this provides an excellent heat barrier, the practice severely reduces engine performance. In addition, its effect is propagated into the plume, which creates regions of varying mixture ratio with attendant variations of thermodynamic and gas dynamic parameters.

Experimental tests of the R-4D engine conducted by NASA-Manned Spacecraft Center resulted in a specific impulse of about 285 sec. One-dimensional adiabatic flame temperature equilibrium calculations by the NASA-Lewis Thermochemical program showed a specific impulse of 337 sec. The difference in specific impulse values are attributed to inefficiencies which reduce the performance of the engines below the maximum energy available from the propellants. Several causes of non-ideal performance have been isolated, for instance: momentum loss because of combustion, O/F maldistribution, kinetic effects and two dimensional effects. These conditions still do not account for the entire performance loss of the engine. The remaining losses are attributed to the inefficiencies in the combustion process.

The ICRPG Committee (Ref. 12) has recommended a method of artificially reducing propellant heats of formation to account for combustion inefficiencies. A dual study of the R-4D was therefore conducted. The standard heat of formation was used in one case and the heat of formation reduced by 250 cal/gm in the other case. The 250 cal/gm was an arbitrary value selected to approximate the experimental I_{sp} value. Loss mechanisms discussed previously were included in both analyses. Only the standard heat of formation case is presented here in order to provide conservative design parameters.

In this analysis several of the loss mechanisms are inherent. The O/F gradient effect, the momentum loss in the combustion process, two-dimensional effects in the transonic and supersonic flow portions of the engine were treated as integral parts of the analysis. The finite-rate effects were treated by an equilibrium/frozen approximation procedure. A parametric variation was done of the freezing point pressure used in the equilibrium/frozen nozzle flow calculations. The effect of location of the freezing point on the predicted I_{sp} was found to be very small (Ref. 13). For extreme cases such as freezing the flow at the throat, the I_{sp} was reduced by 5 percent. Any of the freezing pressure values within the range of selection showed a negligible variation in the predicted I_{sp} value.

3.1 COMBUSTION ANALYSIS

Prior to performing the calculations reported in the main body of this report, a correlation study of the R-4D engine using N_2O_4/A-50 propellants was performed. Experimental data in the form of pitot pressures, heating rates and performance were available which were used, along with injector geometry, to determine mass flow and O/F ratio distributions. A detailed discussion of this auxiliary study is contained in the Appendix. Figure 1 shows a sketch of the R-4D Rocket Engine.

The combustion analysis for N_2O_4/MMH propellants was conducted based on the mixture ratio-mass flow distribution for N_2O_4/A-50 propellants, (see Appendix) and the method of analysis described in Section 2.

An assumption of uniform mass flow per unit area over the entire injector face was made to eliminate severe step gradients in mass flow-mixture ratio due to injector geometry. This assumption was necessary to obtain a physically reasonable solution of the initial combustion process from the Streamtube program. The proper overall mass flow was maintained, but the exact mass flow through the preigniter region could not be matched using this assumption.

Orifice(s)	$\dot{m}$ in lb/sec		O/F	% Fuel in Terms of Total Fuel	% Fuel in Terms of Total Propellant
	ϕ Oxidizer	F Fuel			
Doublet Inside Preigniter	0.061	0.0175	3.47	14.0	4.8
Preigniter Cooling	0.0	0.0169	0.0	13.5	4.7
Main Core Doublet	0.180	0.061	2.96	48.5	17.0
Wall Cooling	0.0	0.030	0.0	24.0	8.3

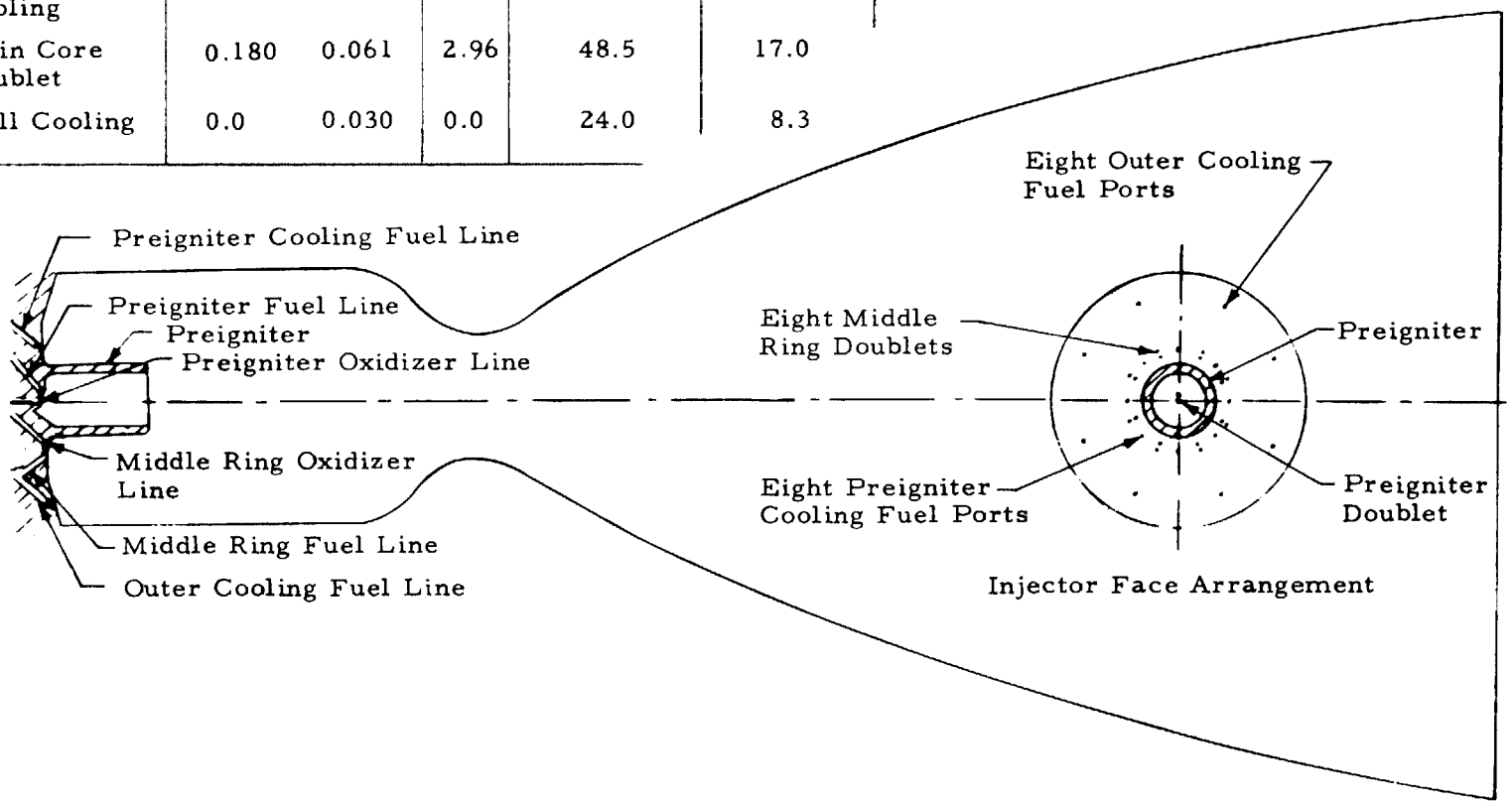

Fig. 1 - Sketch of the R-4D Rocket Engine

The initial O/F ratio distribution across the injector face, based on the preceding discussion plus the assumption of a parabolic shape, is the following:

$$\text{O/F ratio} = 3.5 - 3.76\,r^2$$

where the dimensions of r are inches.

The Streamtube program provided data for the Ducted Equilibrium Mixing program. The velocity, temperature and O/F ratio distributions at the injector after the equilibrium combustion and those at the entrance to the convergent section are shown in Fig. 2. From these results it was concluded that a small amount of mixing occurred through the chamber length. This was the result of the low value of constant viscosity model chosen (6.033×10^{-4} slugs/ft-sec) and because partial mixing had been presumed with the introduction of uniform mass flow per unit area across the injector face.

3.2 TRANSONIC ANALYSIS

The nozzle contour, Fig. 3, used for this analysis was obtained from the Marquardt Corporation. The points from Table 1 were curve-fit by a least-squares technique and the two resulting curves then used as upper boundary conditions in the transonic and the MOC solutions.

$$0 \leq X \leq 0.278$$

$$R = -1.0\left(\sqrt{0.27931 - X^2} - 0.9625\right)$$

$$0.278 \leq X \leq 6.984$$

$$R = -0.000256\,X^4 + 0.0058873\,X^3 - 0.074477\,X^2 + 0.66247\,X + 0.33698$$

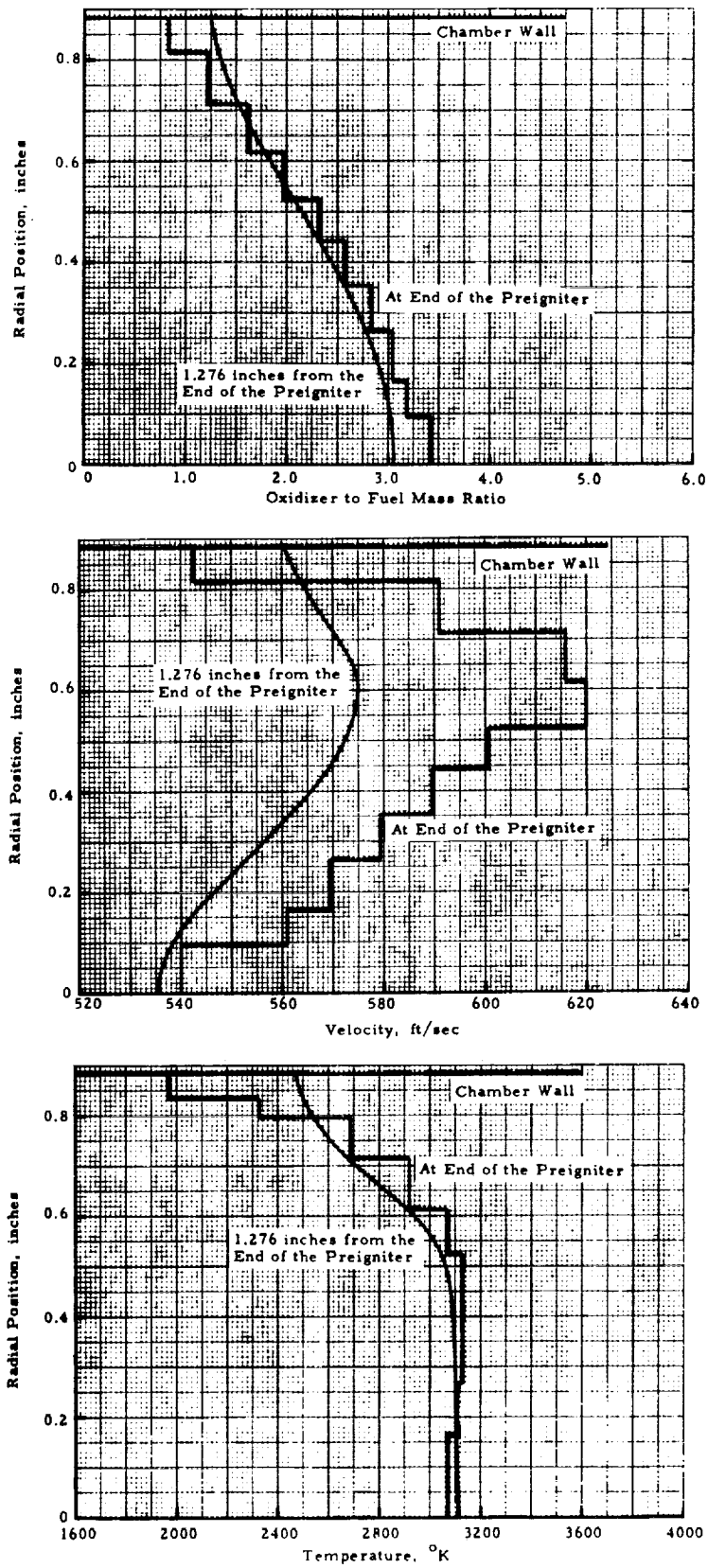

Fig. 2 - Properties at the End of the Preigniter and at the Inlet to the Convergent Section of the Nozzle (1.276 inches from the end of the Preigniter)

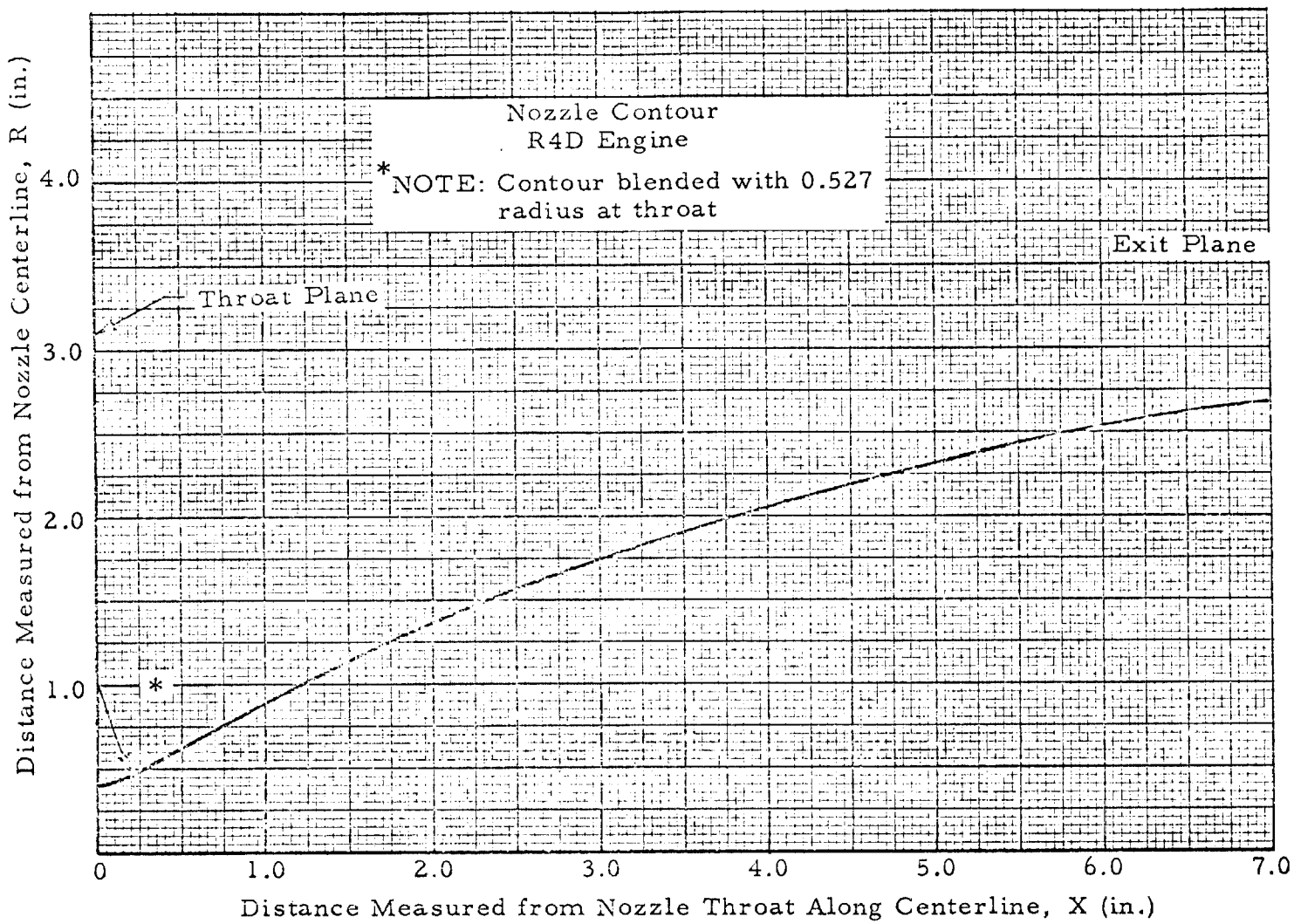

Fig. 3 - Nozzle Contour for R4D

Table 1

NOMINAL R-4D ENGINE OPERATING CHARACTERISTICS FOR COMMAND SERVICE MODULE REACTION CONTROL SYSTEM APPLICATION

Propellant	Engine Parameters
Oxidizer N_2O_4	$A/A^* = 40.0$
Fuel CH_3NHNH_2 (Monomethylhydrazine)	$D_{exit} = 5.46$ in.
	$\Theta_{exit} = 8$ deg
	$P_C = 100$ psia
	$O/F = 2.03 \pm 0.03$
	$\dot{m}_{total} = 0.366\ lb_m/sec$
	Thrust (nominal) $= 100 \pm 5\ lb_f$(vac)
	$D_{chamber} = 1.77$ in.

Nozzle Contour

X	R	
0.000	0.434	Throat – Blend nozzle contour with throat using 0.527 radius of curvature. See Fig. 3.
0.278	0.513	
0.474	0.635	
0.812	0.832	
1.339	1.106	
1.400	1.134	
1.866	1.349	
2.393	1.565	
2.920	1.762	
3.447	1.940	
3.974	2.101	
4.501	2.245	
5.028	2.372	
5.555	2.483	
6.082	2.583	
6.609	2.671	
6.984	2.730	Exit Plane

An unsteady time-dependent finite difference solution procedure was used to describe the transonic flow in the nozzle throat region. Initial conditions consisted of the mixed profiles of the gas dynamic properties at the entrance to the convergent section (Fig. 2). Non-isoenergetic flow was considered (i.e., O/F gradients) as well as equilibrium chemistry throughout the transonic region. Supersonic starting conditions for the MOC program were obtained from the transonic flow description. The Mach number, flow angle and O/F ratio distribution on the starting line are shown in Fig. 4. (See Table 1 for a description of the operating characteristics of the R-4D engine.)

3.3 NOZZLE FREEZING POINTS

The variable O/F MOC program was used to describe the flow field within the nozzle and plume regions. The AeroChem Finite-Rate program was applied to determine the freezing points for the centerline and wall streamlines. The values of freeze pressure were determined by plotting the variation of the constituents along the centerline and wall of the nozzle. The mole fraction variation of the constituents along the centerline of the R-4D nozzle are shown in Fig. 5. The region where there is negligible change in the mole fraction of the constituents is defined as a transition zone from fast (nearly equilibrium) to slow (nearly frozen) reactions. For computational purposes the zone is shrunk to a point (the freezing point). The pressure corresponding to that axial location becomes the freezing pressure. The O/F ratio of 3.07 on the centerline was frozen at 0.008 atmospheres of pressure while the O/F ratio of 1.24 on the wall was frozen at 3.0 atmospheres. The freezing pressure used for the O/F ratios other than those on the centerline and wall was taken as the value obtained by a straight-line variation between the calculated wall and centerline values. Since no practical means was available to determine the freezing point values for the intermediate O/F ratios and any variation chosen was arbitrary, the use of the least confusing straight-line variation seemed appropriate. The final nozzle flow calculation was done using the equilibrium/frozen thermochemical properties shown in Table 2.

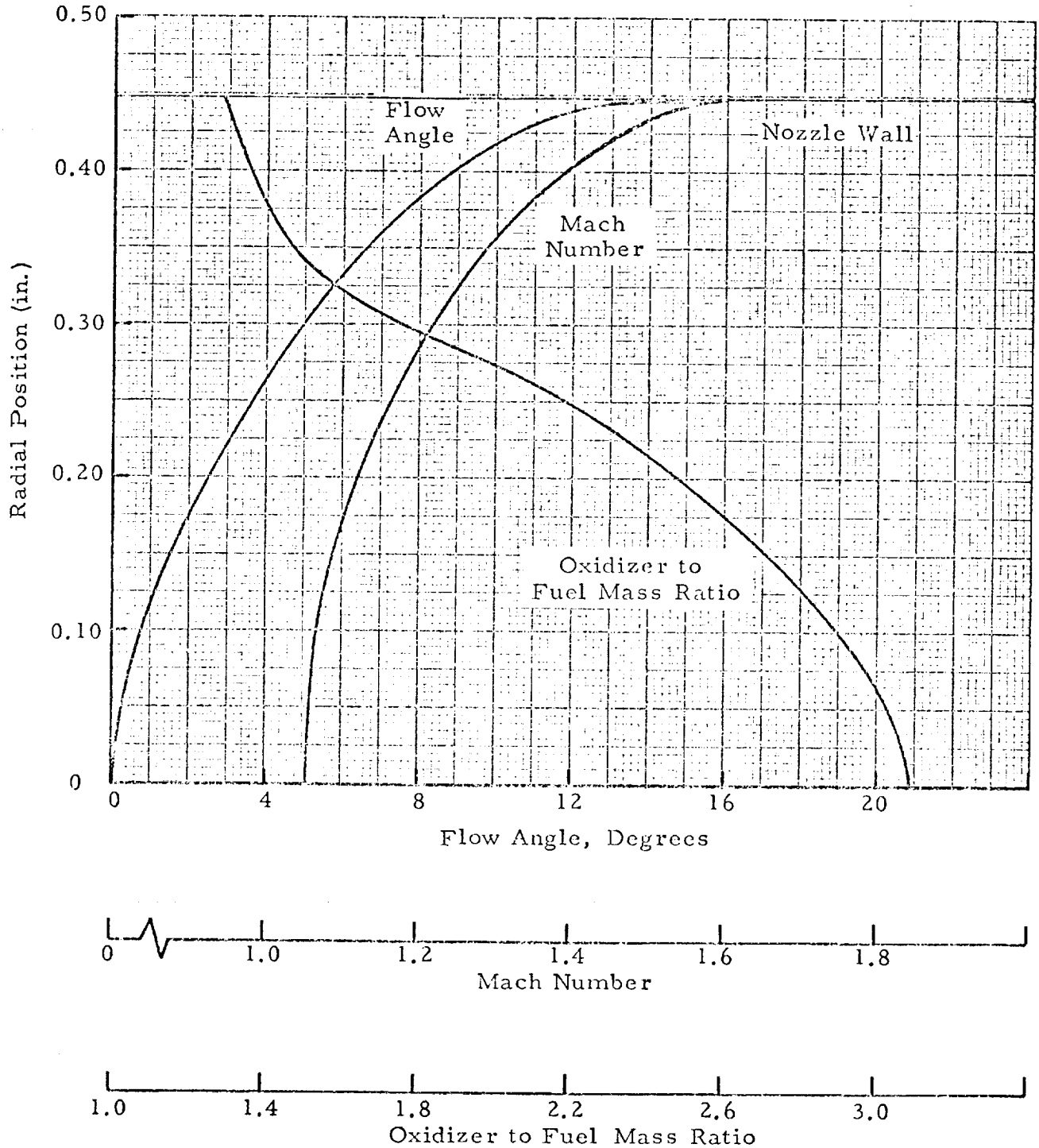

Fig. 4 - Starting Line Conditions for MOC Calculation.
Starting Line at 0.124 in. from Throat.

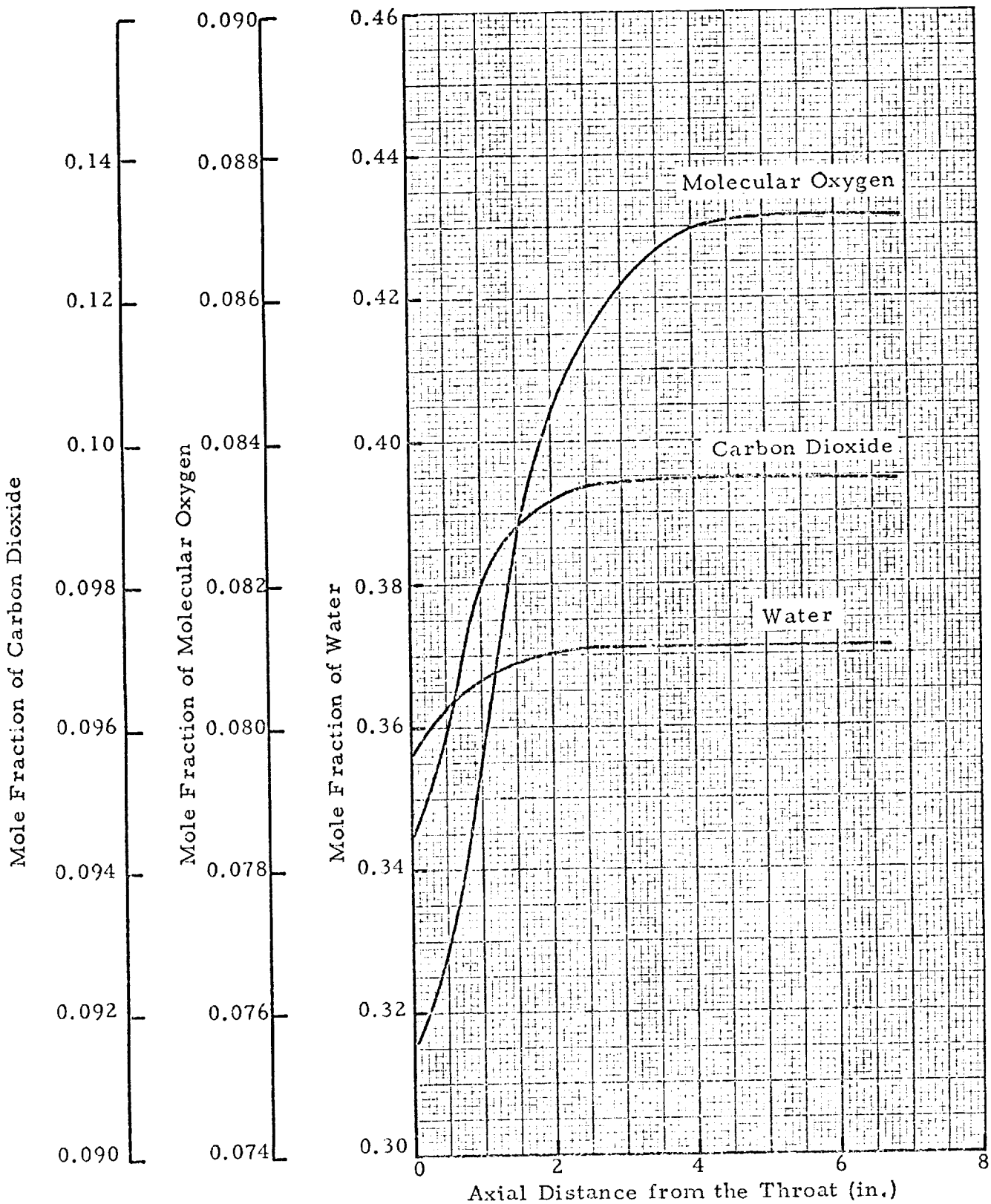

Fig. 5a - Constituent Mole Fraction Variation Along the Centerline of the R-4D Engine Nozzle at an O/F of 3.07 for an MMH/N_2O_4 Propellant System.

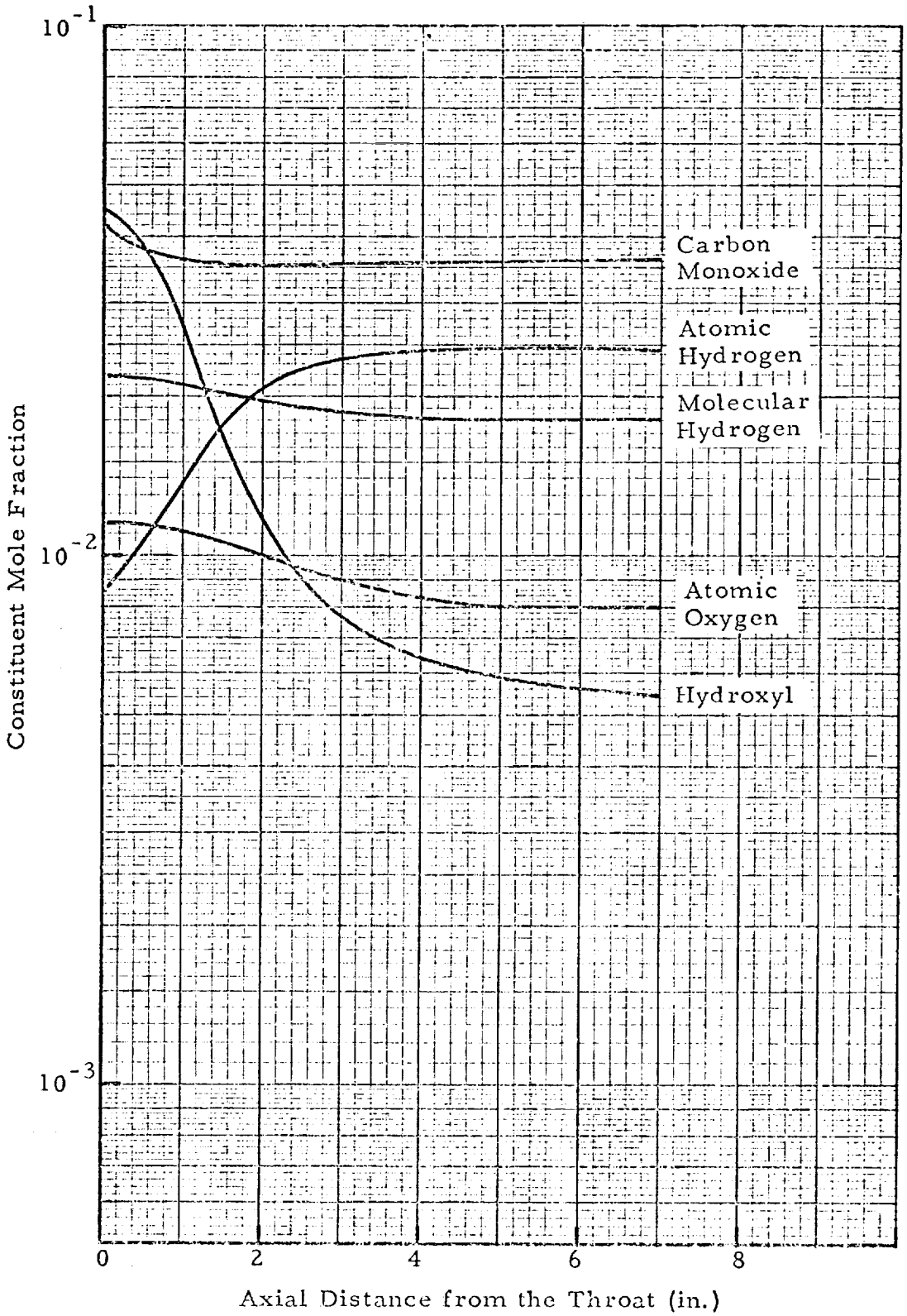

Fig. 5b - Constituent Mole Fraction Variation Along the Centerline of the R-4D Engine Nozzle at an O/F of 3.07 for an MMH/N_2O_4 Propellant System.

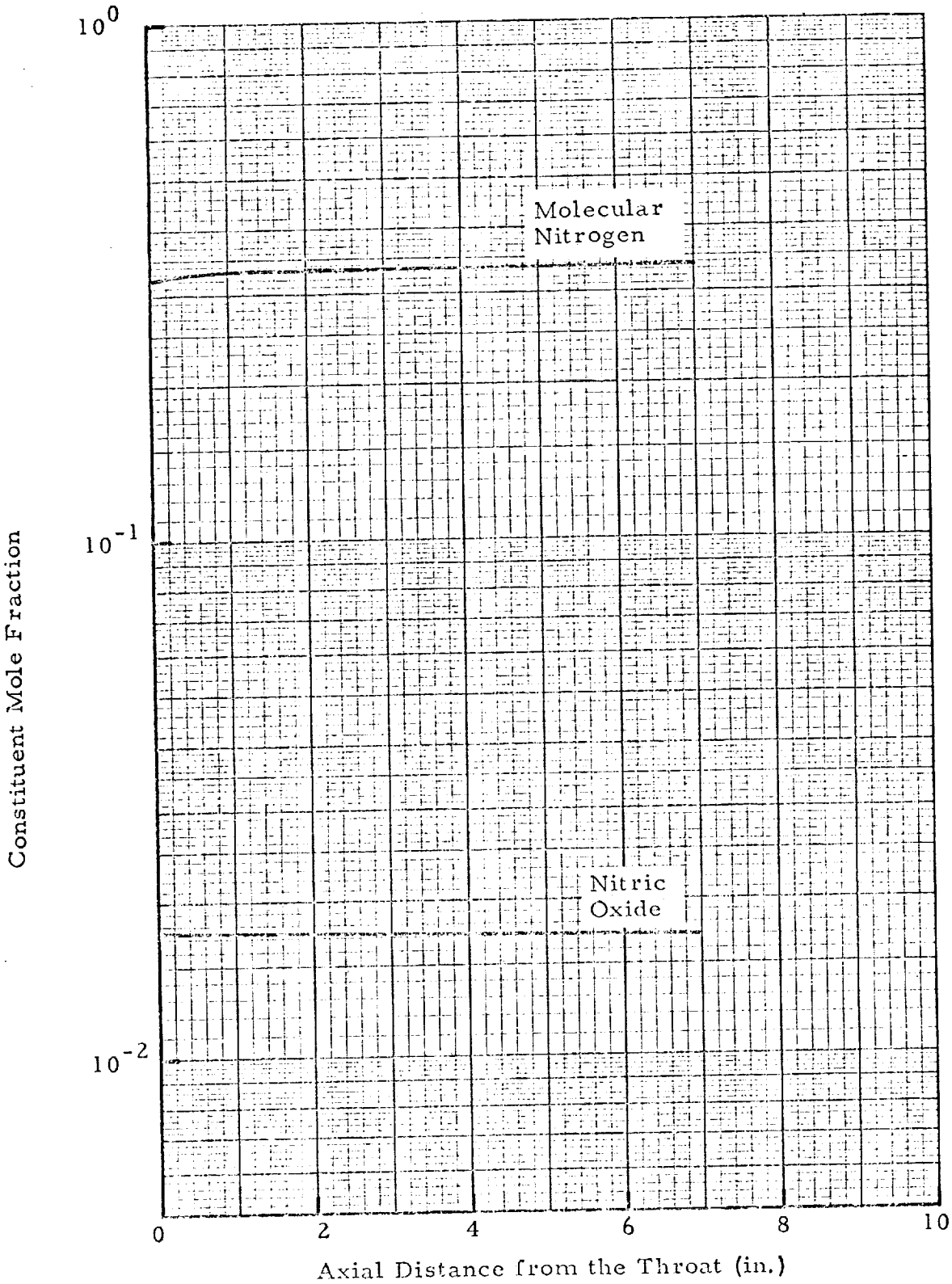

Fig. 5c - Constituent Mole Fraction Variation Along the Centerline of the R-4D Engine Nozzle at an O/F of 3.07 for an MMH/N_2O_4 Propellant System.

THE FOLLOWING GAS PROPERTIES IN ENGLISH UNITS ARE FOR MONOMETHYLHYDRAZINE/NITROGEN TETROXIDE

Table 2

THERMODYNAMIC PROPERTIES OF AN EQUILIBRIUM/FROZEN MONOMETHYLHYDRAZINE/NITROGEN TETROXIDE SYSTEM FOR THE OXIDIZER-TO-FUEL MASS RATIO RANGE OF THE R-4D ENGINE

O/F	S	H	G	T	P
0.10000E 01					
	0.00000E-38				
		0.29725E 04	0.12498E 01	0.42184E 04	0.14400E 05
		0.29693E 04	0.12661E 01	0.37220E 04	0.77838E 04
		0.29690E 04	0.12676E 01	0.36616E 04	0.72000E 04
		0.29690E 04	0.12767E 01	0.36616E 04	0.72000E 04
		0.29690E 04	0.12812E 01	0.34025E 04	0.51429E 04
		0.29690E 04	0.12865E 01	0.31996E 04	0.36000E 04
		0.29690E 04	0.12965E 01	0.27207E 04	0.18947E 04
		0.29690E 04	0.13507E 01	0.13478E 04	0.10667E 03
		0.29690E 04	0.13752E 01	0.82206E 03	0.16744E 02
		0.29690E 04	0.13767E 01	0.76460E 03	0.14117E 02
		0.29690E 04	0.13840E 01	0.58277E 03	0.47996E 01
		0.29690E 04	0.13935E 01	0.26485E 03	0.28781E 00
	0.20863E 05				
		0.30195E 04	0.11572E 01	0.38835E 04	0.14390E 02
		0.29937E 04	0.11830E 01	0.36086E 04	0.81686E 01
0.15000E 01					
	0.00000E-38				
		0.25281E 04	0.11684E 01	0.52839E 04	0.14400E 05
		0.25071E 04	0.11840E 01	0.48401E 04	0.77838E 04
		0.25050E 04	0.11865E 01	0.48053E 04	0.72000E 04
		0.24972E 04	0.11977E 01	0.45661E 04	0.51429E 04
		0.24972E 04	0.12423E 01	0.45661E 04	0.51429E 04
		0.24972E 04	0.12454E 01	0.42577E 04	0.36000E 04
		0.24972E 04	0.12519E 01	0.37470E 04	0.18947E 04
		0.24972E 04	0.12955E 01	0.20268E 04	0.10667E 03
		0.24972E 04	0.13321E 01	0.13025E 04	0.16744E 02
		0.24972E 04	0.13353E 01	0.12480E 04	0.14117E 02
		0.24972E 04	0.13526E 01	0.94673E 03	0.47996E 01
		0.24972E 04	0.13777E 01	0.36835E 03	0.14390E 00
	0.17867E 05				
		0.26476E 04	0.11072E 01	0.43183E 04	0.14390E 02
		0.26114E 04	0.11095E 01	0.41530E 04	0.83803E 01
0.20000E 01					
	0.00000E-38				
		0.22795E 04	0.11323E 01	0.56343E 04	0.14400E 05
		0.22973E 04	0.11321E 01	0.53194E 04	0.77838E 04
		0.22936E 04	0.11322E 01	0.52802E 04	0.72000E 04
		0.22277E 04	0.11337E 01	0.51120E 04	0.51429E 04
		0.22122E 04	0.11369E 01	0.49338E 04	0.36000E 04
		0.22122E 04	0.12249E 01	0.49338E 04	0.36000E 04
		0.22122E 04	0.12295E 01	0.43812E 04	0.18947E 04
		0.22122E 04	0.12625E 01	0.24915E 04	0.10667E 03
		0.22122E 04	0.12955E 01	0.16649E 04	0.16744E 02
		0.22122E 04	0.12989E 01	0.16011E 04	0.14117E 02
		0.22122E 04	0.13200E 01	0.12407E 04	0.47996E 01
		0.22122E 04	0.13639E 01	0.50398E 03	0.14390E 00
	0.16250E 05				
		0.24201E 04	0.10965E 01	0.44110E 04	0.14390E 02
		0.23850E 04	0.10948E 01	0.42718E 04	0.84437E 01
0.22500E 01					
	0.00000E-38				
		0.21967E 04	0.11276E 01	0.56580E 04	0.14400E 05
		0.21642E 04	0.11250E 01	0.53606E 04	0.77838E 04
		0.21602E 04	0.11248E 01	0.53241E 04	0.72000E 04
		0.21436E 04	0.11240E 01	0.51694E 04	0.51429E 04
		0.21266E 04	0.11236E 01	0.50096E 04	0.36000E 04
		0.20988E 04	0.11249E 01	0.47293E 04	0.18947E 04
		0.20988E 04	0.12196E 01	0.47293E 04	0.18947E 04
		0.20988E 04	0.12476E 01	0.27516E 04	0.10667E 03
		0.20988E 04	0.12769E 01	0.18746E 04	0.16744E 02
		0.20988E 04	0.13007E 01	0.14170E 04	0.47996E 01
		0.20988E 04	0.13465E 01	0.71026E 03	0.28781E 00
		0.20988E 04	0.13537E 01	0.59341E 03	0.14390E 00
	0.15677E 05				
		0.23361E 04	0.10952E 01	0.44144E 04	0.14390E 02
		0.23023E 04	0.10932E 01	0.42781E 04	0.84437E 01
0.25000E 01					
	0.00000E-38				
		0.21305E 04	0.11261E 01	0.56378E 04	0.14400E 05
		0.20991E 04	0.11231E 01	0.53454E 04	0.77838E 04
		0.20953E 04	0.11228E 01	0.53096E 04	0.72000E 04
		0.20791E 04	0.11217E 01	0.51584E 04	0.51429E 04
		0.20627E 04	0.11208E 01	0.50028E 04	0.36000E 04
		0.20349E 04	0.11202E 01	0.47331E 04	0.18947E 04
		0.20349E 04	0.12179E 01	0.47331E 04	0.18947E 04
		0.20349E 04	0.12451E 01	0.27645E 04	0.10667E 03
		0.20349E 04	0.12735E 01	0.18898E 04	0.16744E 02
		0.20349E 04	0.12968E 01	0.14325E 04	0.47996E 01
		0.20349E 04	0.13435E 01	0.72225E 03	0.28781E 00
		0.20349E 04	0.13512E 01	0.60403E 03	0.14390E 00
	0.15202E 05				
		0.22654E 04	0.10947E 01	0.44063E 04	0.14390E 02
		0.22328E 04	0.10927E 01	0.42708E 04	0.84437E 01
0.30000E 01					
	0.00000E-38				
		0.20309E 04	0.11268E 01	0.55369E 04	0.14400E 05
		0.20030E 04	0.11249E 01	0.52413E 04	0.77838E 04
		0.19996E 04	0.11248E 01	0.52049E 04	0.72000E 04
		0.19854E 04	0.11244E 01	0.50503E 04	0.51429E 04
		0.19711E 04	0.11247E 01	0.48899E 04	0.36000E 04
		0.19477E 04	0.11272E 01	0.46064E 04	0.18947E 04
		0.18921E 04	0.12051E 01	0.32172E 04	0.10667E 03
		0.18903E 04	0.12467E 01	0.22811E 04	0.16744E 02
		0.18903E 04	0.12478E 01	0.22811E 04	0.16744E 02
		0.18903E 04	0.12674E 01	0.17665E 04	0.47996E 01
		0.18903E 04	0.13181E 01	0.93431E 03	0.28781E 00
		0.18903E 04	0.13291E 01	0.78863E 03	0.14390E 00
	0.19460E 05				
		0.21531E 04	0.10948E 01	0.43724E 04	0.14390E 02
		0.21229E 04	0.10930E 01	0.42359E 04	0.84437E 01

3.4 NOZZLE AND PLUME CALCULATION

Nozzle and plume calculations were performed as described in Section 2. Since the MOC program will handle only one shock wave at a time, the nozzle calculation was terminated when the internal shock intersected the axis. The problem was then inverted and the plume flow field was generated, using downstream shock points and nozzle exit plane points as a start line (Table 3). The plume was allowed to expand into a quasi-vacuum and the effects of the nozzle boundary layer were included. Because of the large expansions encountered, a characteristic mesh control was imposed on the solution to prevent divergence problems. The maximum mesh size permitted was 20 in. measured along any side of a Mach quadralateral. The effect of the boundary layer was to cause a greater expansion due to the lower lip Mach number of the boundary layer.

Table 3

PLUME STARTING LINE PROPERTIES

STARTING LINE

R	X	M	THETA	S	O/F
.00000	.81706+01	.41359+01	.16411+02	.10427+04	.30600+01
-.70000-02	.81620+01	.42700+01	.14600+02	.81700+03	.30582+01
-.14000-01	.81500+01	.43750+01	.13200+02	.66100+03	.30563+01
-.23500-01	.81240+01	.44800+01	.11800+02	.51800+03	.30532+01
-.37500-01	.80830+01	.45908+01	.10400+02	.38600+03	.30479+01
-.60428-01	.80076+01	.46893+01	.91554+01	.28294+03	.30455+01
-.90000-01	.79130+01	.47679+01	.82030+01	.22200+03	.30305+01
-.14052+00	.77304+01	.48488+01	.68893+01	.14956+03	.30248+01
-.19276+00	.75304+01	.48683+01	.55979+01	.11046+03	.30112+01
-.24391+00	.73205+01	.48688+01	.45458+01	.85964+02	.29975+01
-.34186+00	.69167+01	.48262+01	.25844+01	.53456+02	.29663+01
-.53038+00	.71480+01	.47852+01	.11371+01	.24516+02	.28858+01
-.67852+00	.70674+01	.47374+01	.65649-01	.14420+02	.28250+01
-.83143+00	.71190+01	.47533+01	-.12933+01	.83803+01	.27606+01
-.97760+00	.70997+01	.47467+01	-.22685+01	.46639+01	.26959+01
-.11880+01	.70702+01	.46834+01	-.34540+01	.16392+01	.25916+01
-.13891+01	.69650+01	.46024+01	-.45319+01	.35095+00	.24721+01
-.15127+01	.69725+01	.45822+01	-.51954+01	.11745+00	.23927+01
-.16358+01	.69577+01	.45833+01	-.59645+01	.39184-01	.23098+01
-.18238+01	.68801+01	.44650+01	-.60597+01	.72613-01	.21620+01
-.20609+01	.69246+01	.44292+01	-.68417+01	.11828-02	.19626+01
-.22664+01	.68455+01	.43463+01	-.74834+01	.25112-03	.17571+01
-.25993+01	.69840+01	.41885+01	-.76787+01	.32927-02	.12800+01
-.26085+01	.69840+01	.37795+01	-.76787+01	.16924+04	.12800+01
-.26174+01	.69840+01	.34529+01	-.76787+01	.31139+04	.12800+01
-.26261+01	.69840+01	.31800+01	-.76787+01	.43332+04	.12800+01
-.26345+01	.69840+01	.29475+01	-.76787+01	.53954+04	.12800+01
-.26426+01	.69840+01	.27428+01	-.76787+01	.63319+04	.12800+01
-.26504+01	.69840+01	.25602+01	-.76787+01	.71655+04	.12800+01
-.26580+01	.69840+01	.23954+01	-.76787+01	.79131+04	.12800+01
-.26653+01	.69840+01	.22450+01	-.76787+01	.85876+04	.12800+01
-.26723+01	.69840+01	.21065+01	-.76787+01	.91991+04	.12800+01
-.26791+01	.69840+01	.19781+01	-.76787+01	.97557+04	.12800+01
-.26855+01	.69840+01	.18583+01	-.76787+01	.10264+05	.12800+01
-.26917+01	.69840+01	.17454+01	-.76787+01	.10729+05	.12800+01
-.26977+01	.69840+01	.16384+01	-.76787+01	.11156+05	.12800+01
-.27033+01	.69840+01	.15368+01	-.76787+01	.11547+05	.12800+01
-.27087+01	.69840+01	.14397+01	-.76787+01	.11907+05	.12800+01
-.27138+01	.69840+01	.13605+01	-.76787+01	.12238+05	.12800+01
-.27186+01	.69840+01	.12724+01	-.76787+01	.12542+05	.12800+01
-.27232+01	.69840+01	.11868+01	-.76787+01	.12821+05	.12800+01
-.27274+01	.69840+01	.11036+01	-.76787+01	.13076+05	.12800+01

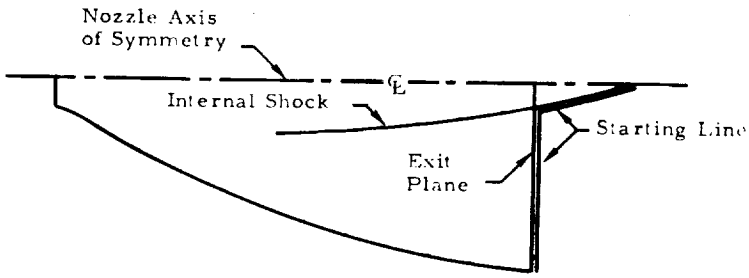

Section 4
PRESENTATION OF RESULTS

4.1 DISCUSSION OF RESULTS

The results of the study are presented in terms of plume parameters as a function of spatial location, i.e., contour plots, as well as centerline property distributions within the plume. Tables of thermochemical properties used in the generation of the plume are also presented.

The distribution of mass flow in the plume is shown in Fig. 6. Each streamline represents a percentage of the total mass flow contained in the region between the streamline and the centerline. Contour maps of the plume properties, i.e., Mach number, temperature, pressure, density, flow angle, pitot pressure and O/F ratio are presented in Figs. 7 through 13. It can be seen that these contour plots are not the smooth patterned curves normally presented for plume calculations. It should be recalled, however, that in keeping with the study objective, every calculable effect was taken into account in generating the detailed plume properties presented herein. It is not surprising, therefore, to expect slight irregularities in the contour plots arising from such effects as O/F gradients, entropy gradients (due to shock waves), nozzle wall boundary layer, and the nozzle contour itself, which gives rise to additional compressions in the flow field.

In addition to the contour maps, plots of the centerline distributions of the plume parameters are presented in Figs. 14 through 17. The pitot pressures presented in Fig. 15 should aid in comparing experimental data which usually consists of pitot pressure measurements along the centerline.

As discussed in Section 2.4.1, continuum analyses were used throughout the flow field. To obtain an indication of where non-continuum effects may

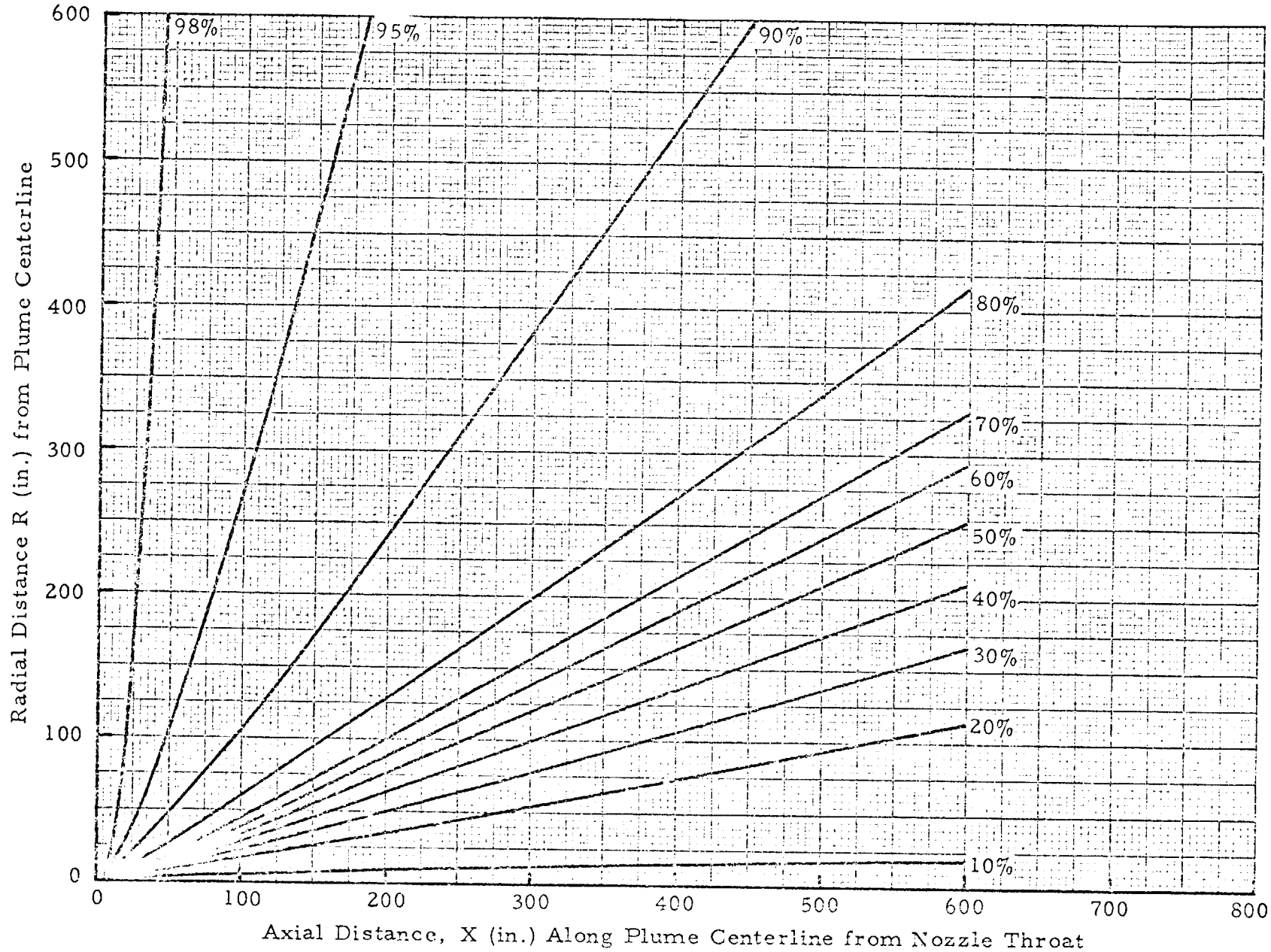

Fig. 6 - Location of Streamlines and Mass Flow Distribution (Percent of Total) in R-4D Plume Flowfield

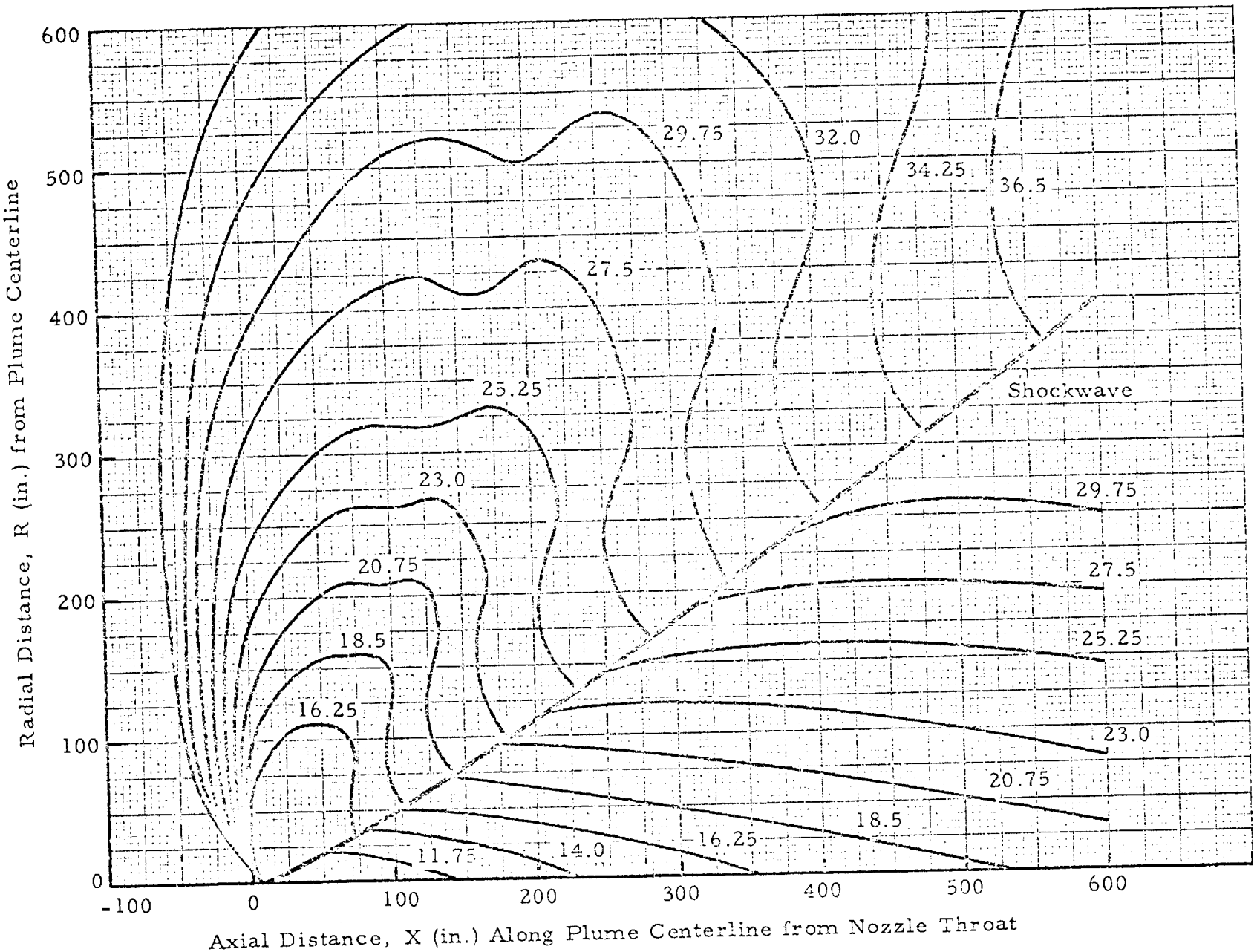

Fig. 7 - Lines of Constant Mach Number in R-4D Plume Flowfield

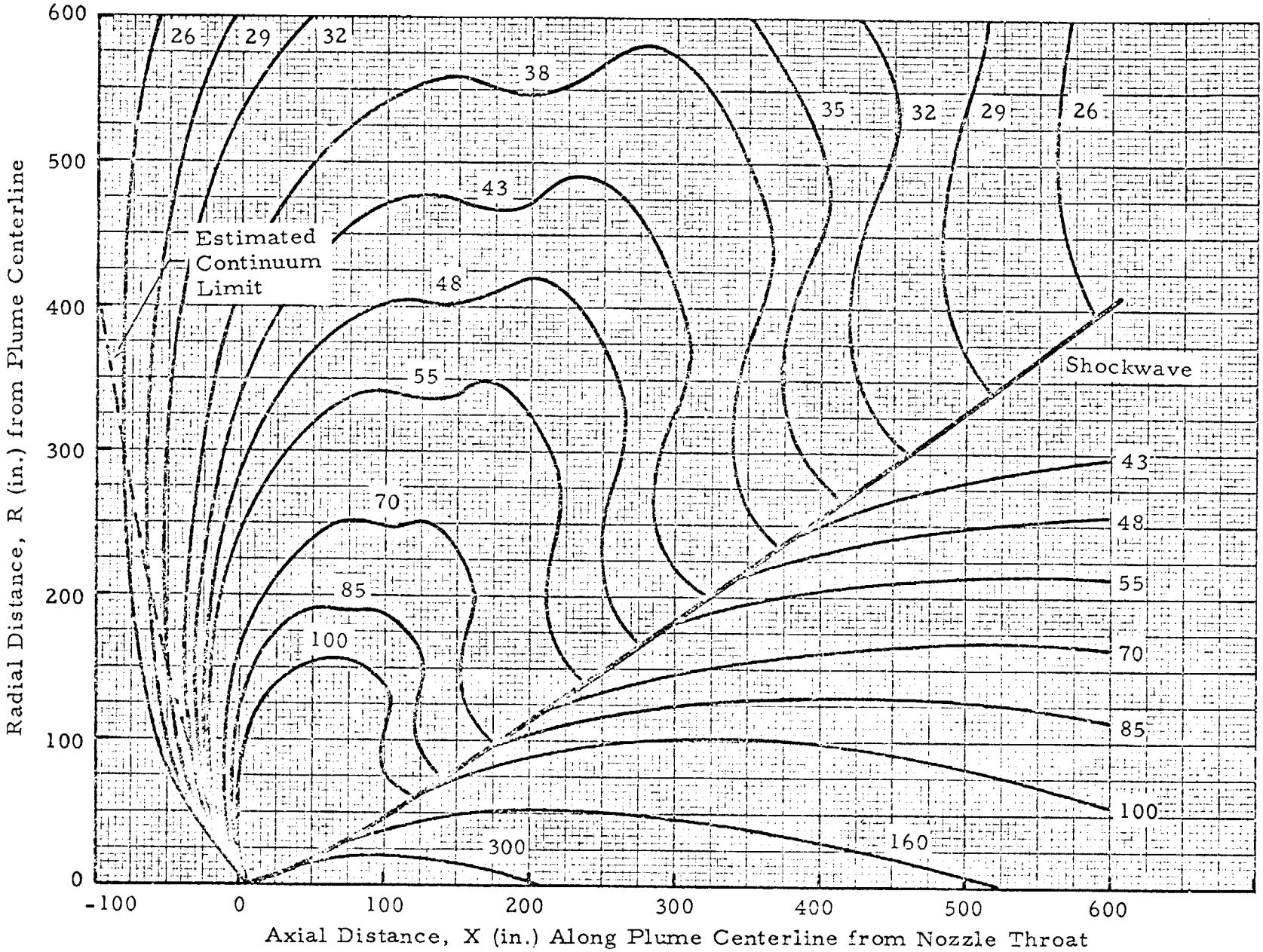

Fig. 8 - Lines of Constant Temperature (^{o}R) in R-4D Plume Flowfield

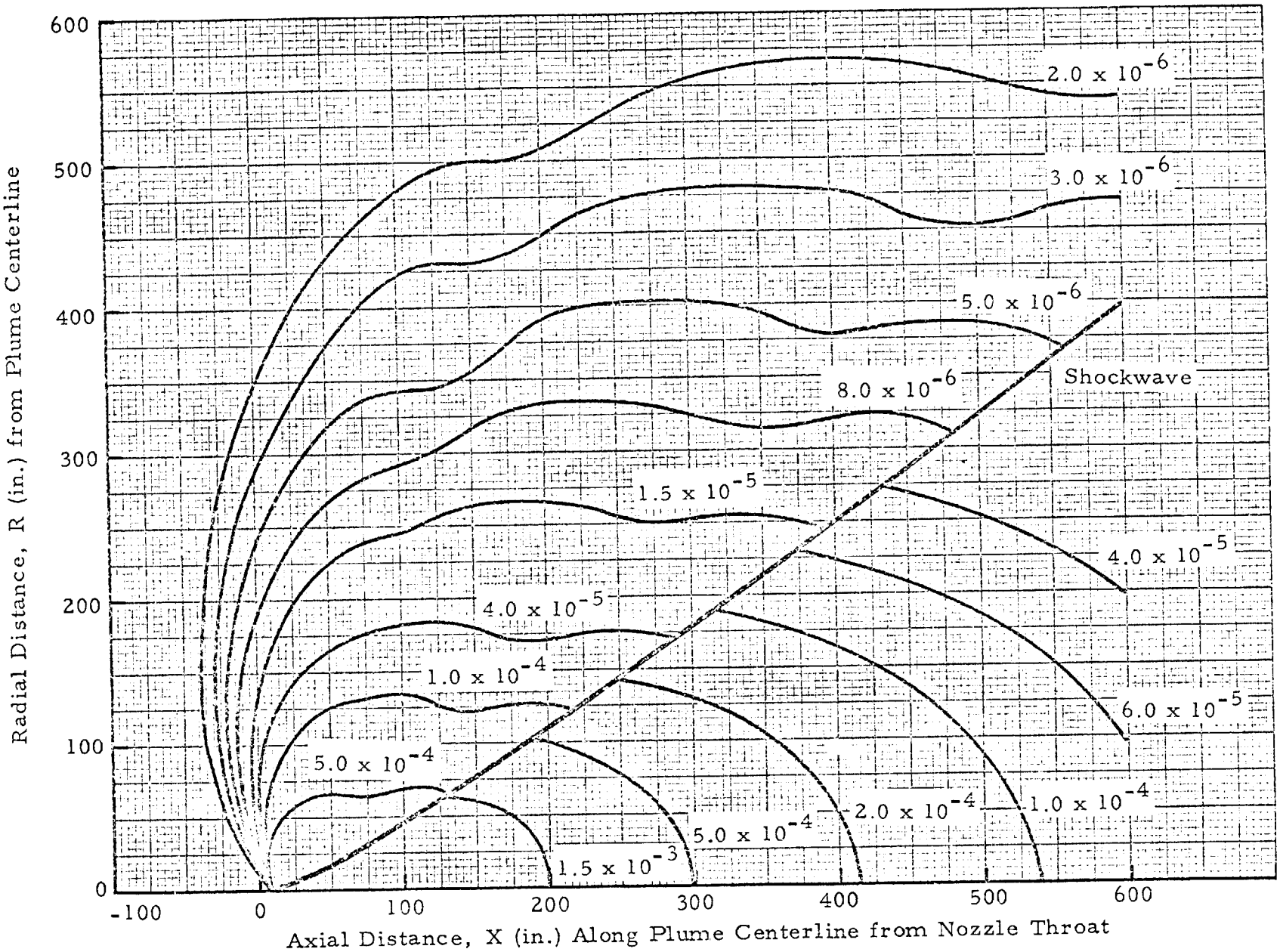

Fig. 9 - Lines of Constant Static Pressure (psfa) in R-4D Plume Flowfield

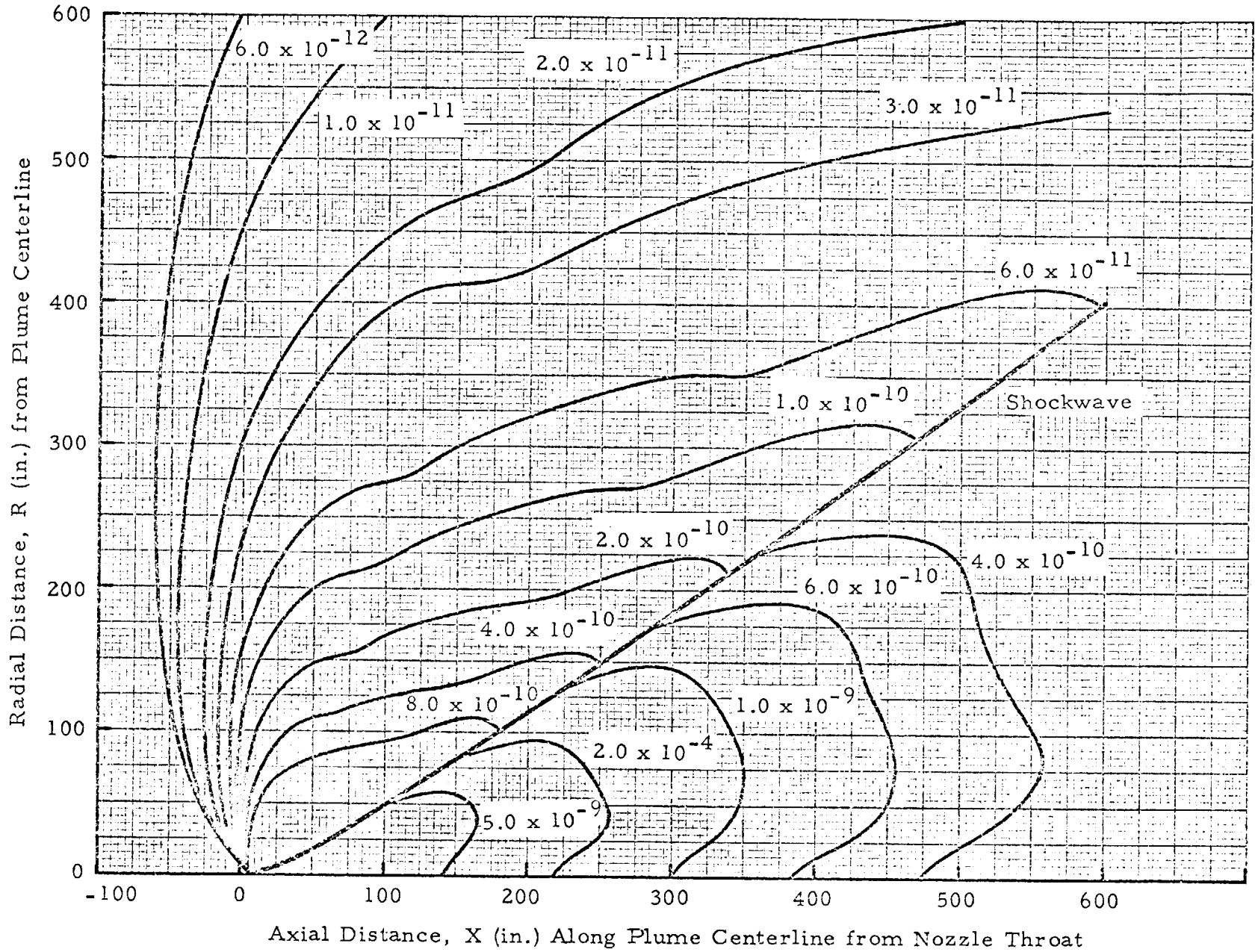

Fig. 10 - Lines of Constant Density (slugs/ft^3) in R-4D Plume Flowfield

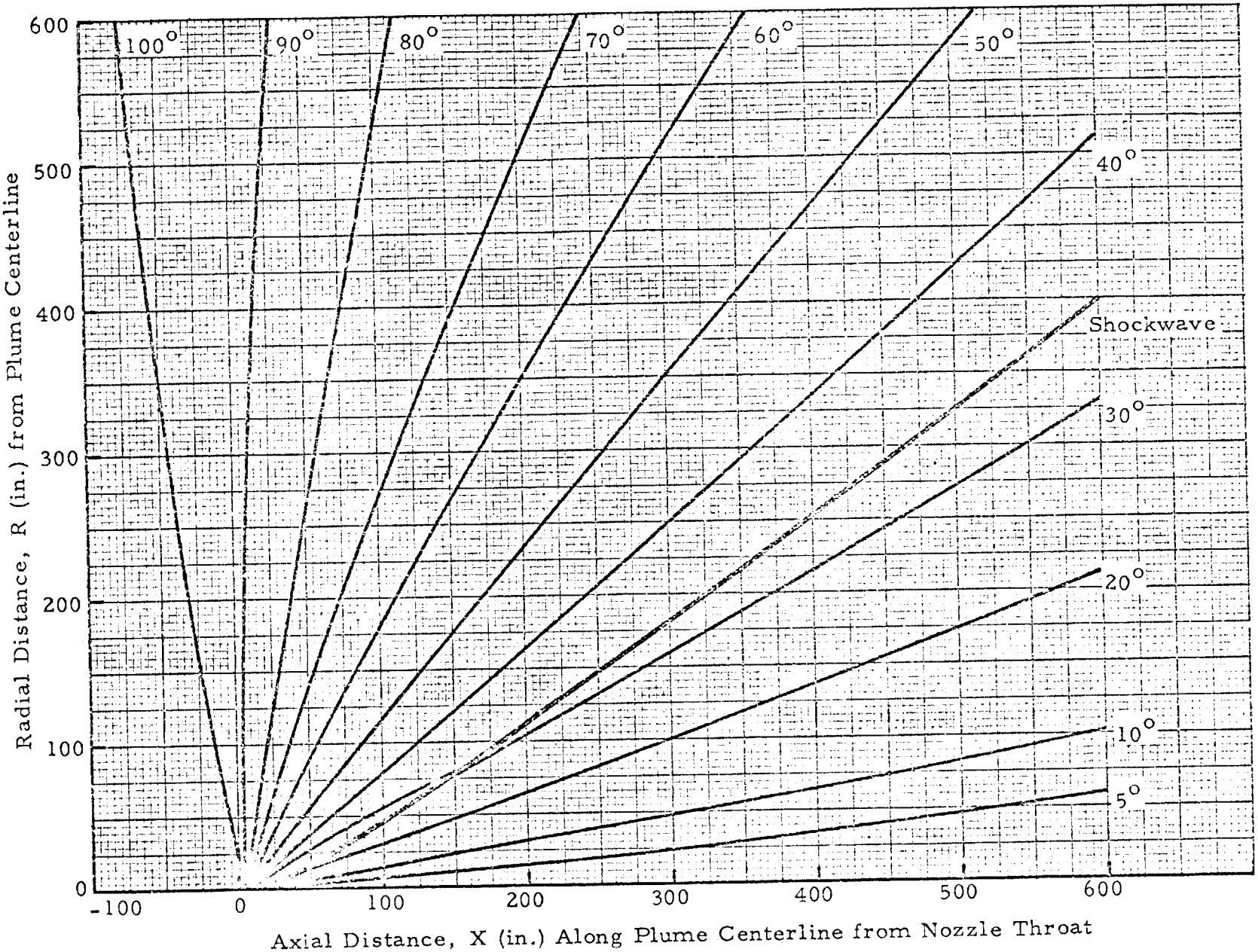

Fig. 11 - Lines of Constant Flow Angle (degrees) in R-4D Plume Flowfield

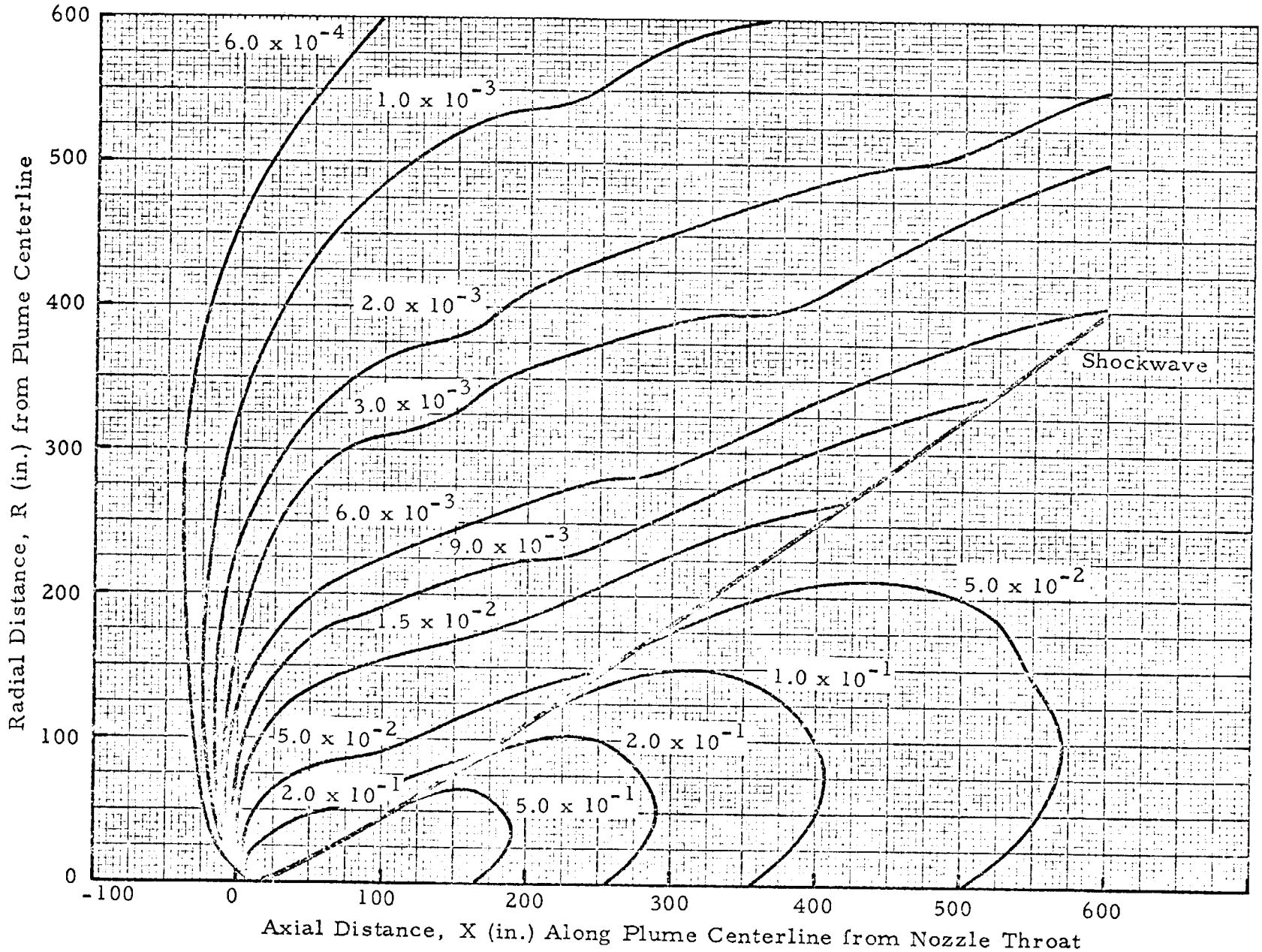

Fig. 12 - Lines of Constant Pitot Pressure (psfa) in the R-4D Plume Flowfield

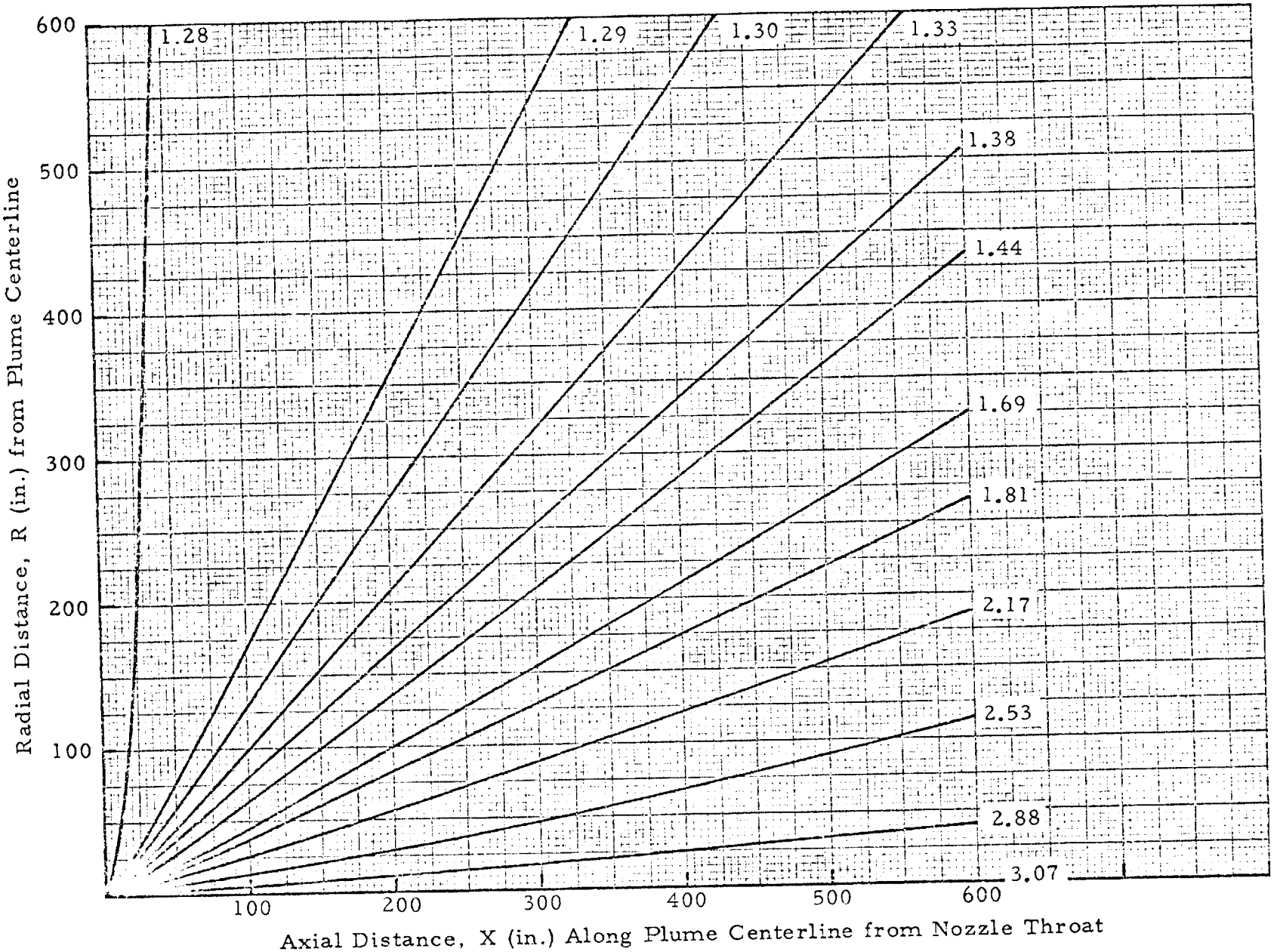

Fig. 13 - Lines of Constant O/F Ratio in R-4D Plume Flowfield

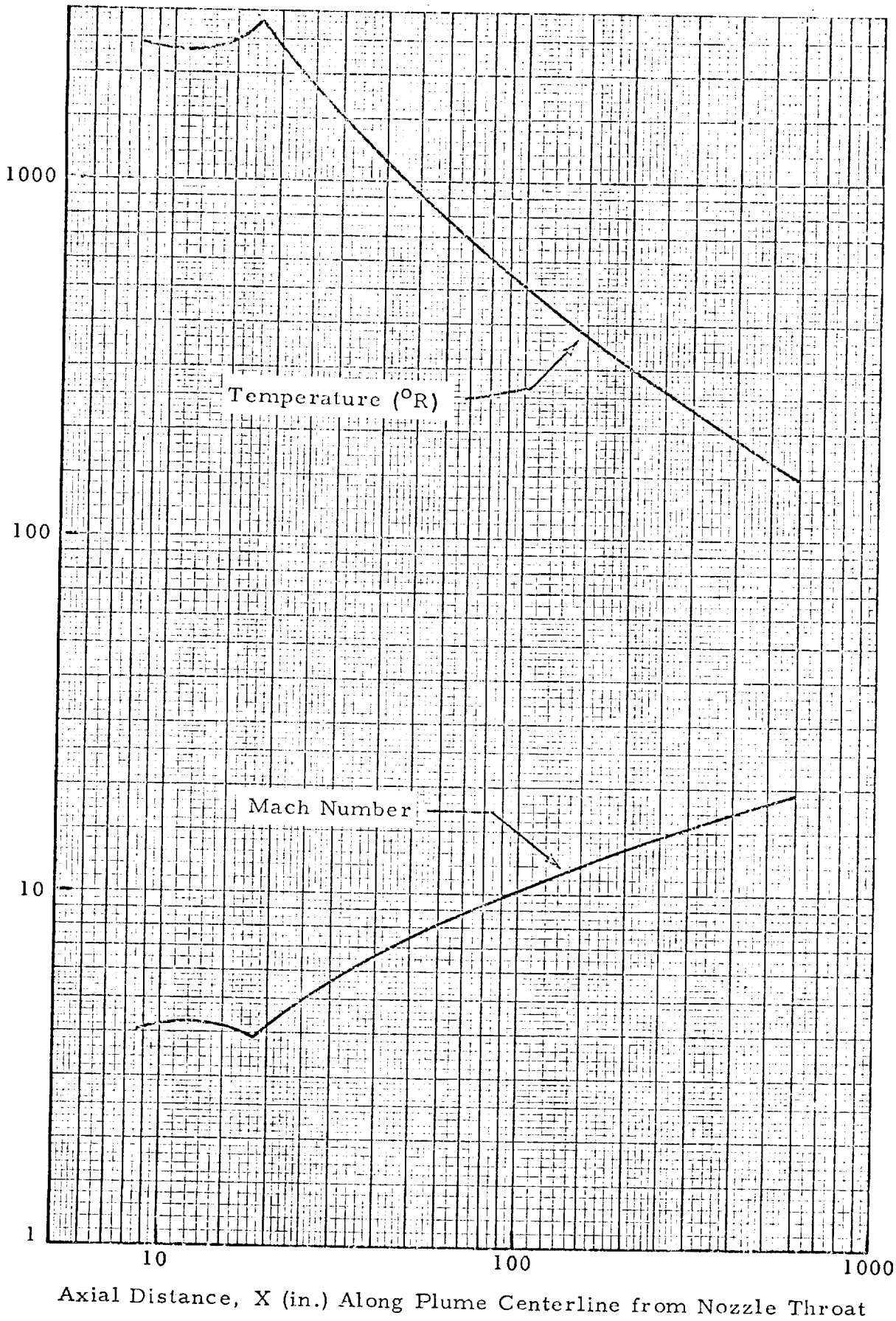

Fig. 14 - Mach Number and Temperature Distribution Along Centerline of R-4D Plume Flowfield

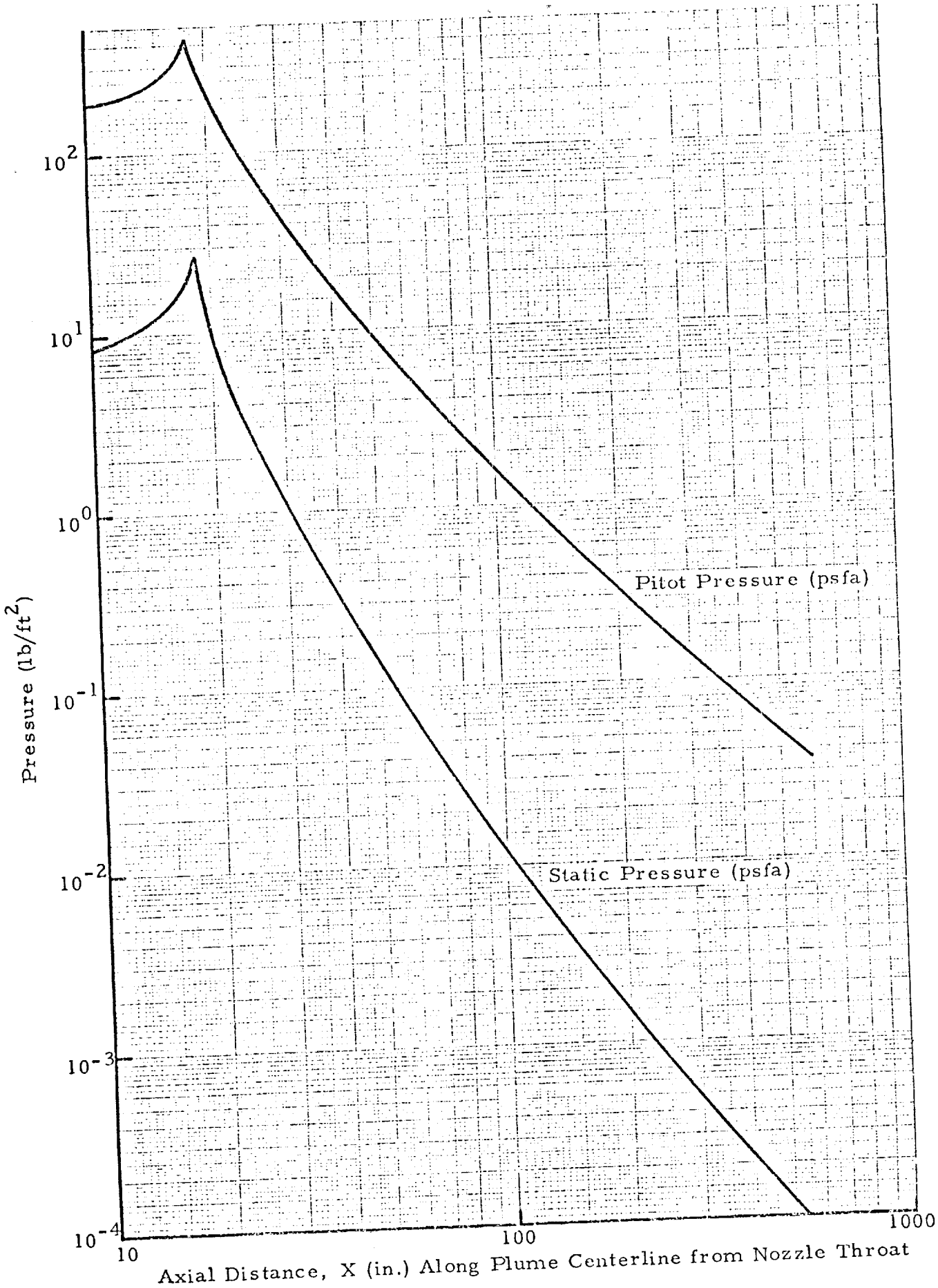

Fig. 15 - Pitot and Static Pressure Distribution Along Centerline of R-4D Plume Flowfield

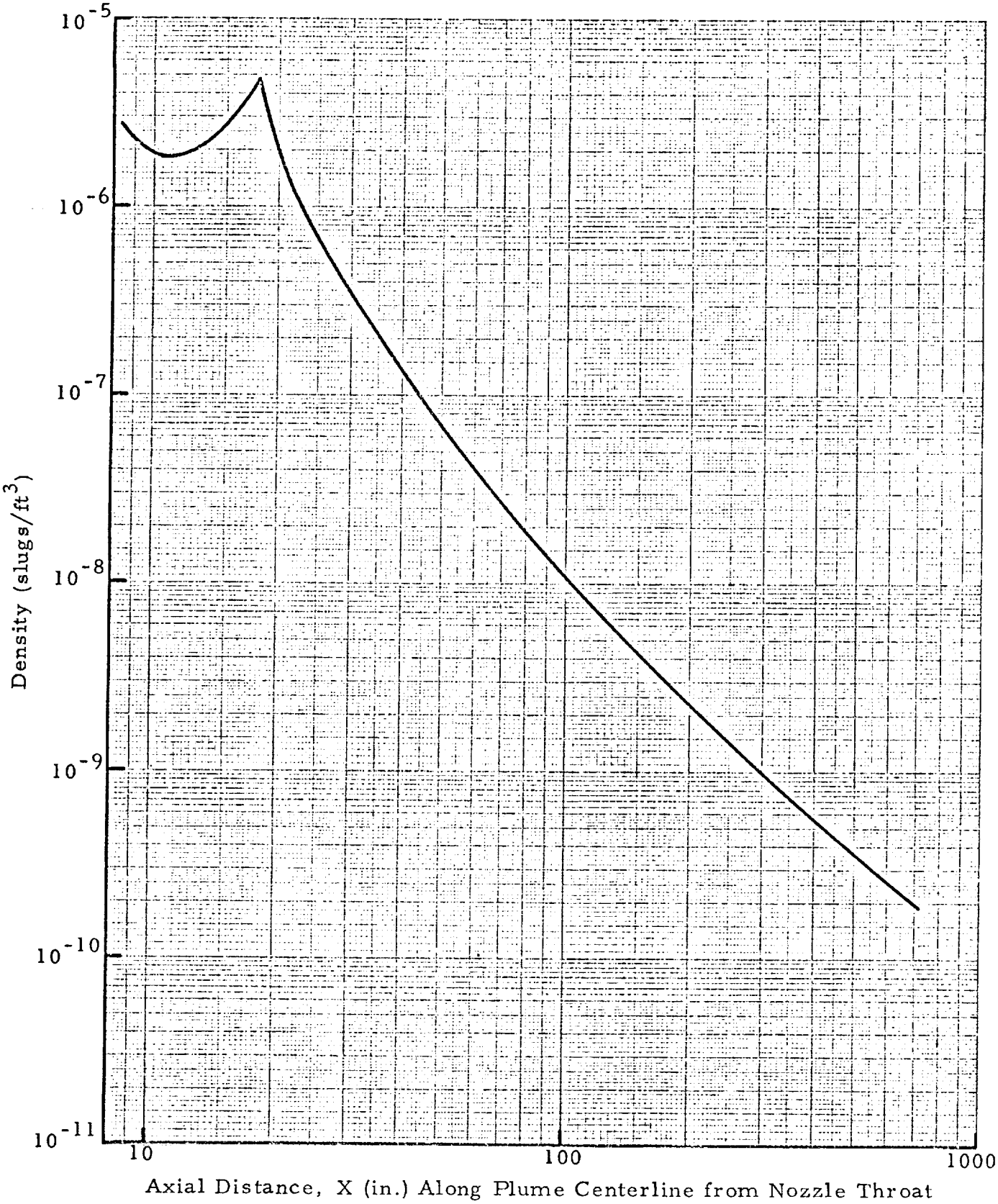

Fig. 16 - Density Distribution Along Centerline of R-4D Plume Flowfield

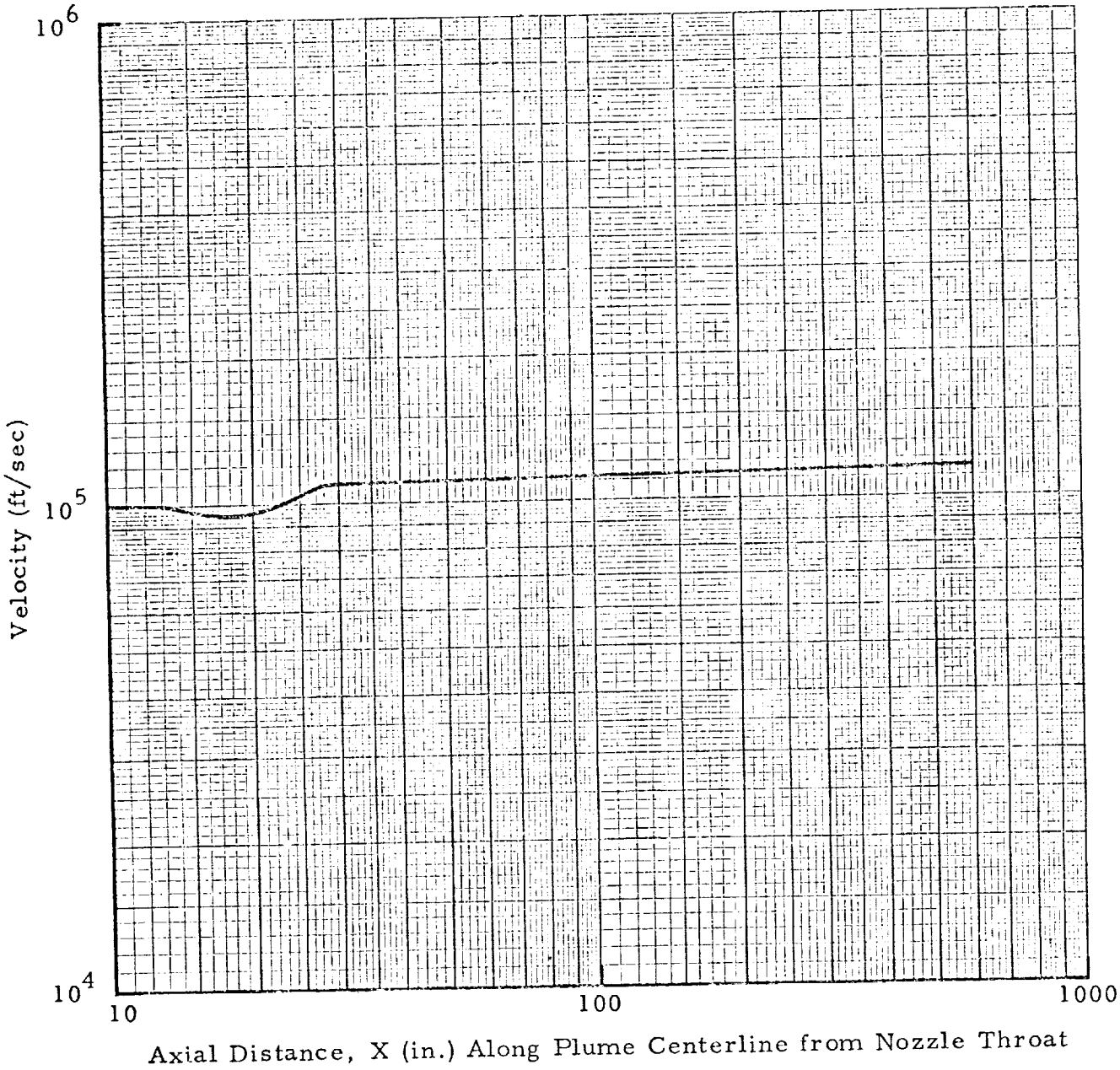

Fig. 17 - Velocity Distribution Along Centerline of R-4D Plume Flowfield

become detectable, however, the translational "freeze" line based on a Knudsen number criterion of 1.0 was computed and is shown on the temperature contour plot, Fig. 8. The major deviation caused by non-continuum effects would be in the streamwise temperature component which would be somewhat higher, in the region above the "freeze" line, than the continuum calculations shown in Fig. 8.

Since the kinetics analysis, previously discussed, indicated that the flowfield chemistry was frozen inside the nozzle, the entire plume was computed using frozen chemistry. The species present in the plume as a function of O/F ratio are presented in Table 4.

4.2 SUMMARY OF RESULTS

The plume flow field of the R-4D motor was analytically generated, the analysis starting at the injector and continuing through the combustion chamber, the subsonic and supersonic nozzle sections, and 50 feet into the plume region. To provide the basic information needed for doing impingement analyses, the plume data were generated to be as detailed as possible including all the existing calculation procedures to treat the physical phenomena present. The momentum loss because of combustion, O/F maldistribution, kinetic effects and two-dimensional effects which cause non-ideal engine performance were treated as integral parts of the analysis. The possibility of condensation was considered but incipient condensation or calculation of a multi-phase plume flow field was not treated in this analysis. The effect on the plume flow field of nozzle boundary layer and internal shocks appeared in the plots of physical properties of the plume. While the plots of the flow properties contain certain irregularities not present in a more simplified plume analysis, these irregularities were found to be present when every calculable effect in the flow was treated in generating the plume properties. When detailed impingement analyses are required, the inclusion of all the calculable effects was therefore concluded to be necessary and worthy of the increased time and effort.

Table 4

CONSTITUENT MOLE FRACTIONS AT THE FREEZING POINT PRESSURES FOR THE R-4D ENGINE NOZZLE FLOW WITH AN O/F VARIATION FROM 1.24 TO 3.07 WITH AN N_2O_4/MMH PROPELLANT SYSTEM

O/F Ratio	1.240	1.290	1.300	1.330	1.380	1.440
CO	0.15345	0.15204	0.15147	0.14975	0.14674	0.14294
CO_2	0.02404	0.02462	0.02501	0.02619	0.02829	0.03099
H	0.00256	0.00440	0.00458	0.00516	0.00615	0.00748
H_2	0.28853	0.27303	0.26958	0.25927	0.24241	0.22262
H_2C	0.24250	0.25436	0.25717	0.26547	0.27893	0.29439
NO	0.00002	0.00005	0.00005	0.00007	0.00010	0.00016
N_2	0.28857	0.29074	0.29133	0.29307	0.29594	0.29926
O	0.00000	0.00001	0.00001	0.00001	0.00002	0.00005
OH	0.00032	0.00074	0.00079	0.00100	0.00140	0.00207
O_2	0.00000	0.00000	0.00000	0.00001	0.00001	0.00003

O/F Ratio	1.636	1.814	2.170	2.526	2.882	3.070
CO	0.12861	0.11302	0.07754	0.04338	0.00860	0.00000
CO_2	0.04160	0.05360	0.08144	0.10778	0.13617	0.14272
H	0.01163	0.01408	0.01255	0.00695	0.00099	0.00000
H_2	0.16313	0.11803	0.05766	0.02607	0.00507	0.00000
H_2O	0.33876	0.36910	0.40147	0.41113	0.42282	0.42815
NO	0.00062	0.00155	0.00462	0.00695	0.00482	0.00014
N_2	0.30933	0.31720	0.32940	0.33886	0.35127	0.35705
O	0.00027	0.00087	0.00320	0.00443	0.00161	0.00000
OH	0.00582	0.01141	0.02301	0.02559	0.01182	0.00004
O_2	0.00023	0.00112	0.00912	0.02885	0.05682	0.07190

REFERENCES

1. Ratliff, A. W., and J. T. Stephens, "A Detailed Plume Flowfield Definition of the R-1E Motor for the Saturn S-IVB Auxiliary Propulsion System," LMSC/HREC D148776, Lockheed Missiles & Space Company, Huntsville, Ala., June 1969.

2. Prozan, R. J., "Striated Combustion Solution," LMSC/HREC A791356, Lockheed Missiles & Space Company, Huntsville, Ala., May 1968.

3. Letter to Mr. David Seymour (NASA-Marshall Space Flight Center) from Dr. Raymond Edelman (General Applied Science Laboratories) 29 October 1968.

4. Prozan, R. J., "Development of a Method-of-Characteristics Solution for Supersonic Flow of an Ideal, Frozen, or Equilibrium Reacting Gas Mixture," LMSC/HREC D782535-A, Lockheed Missiles & Space Company, Huntsville, Ala., April 1966.

5. McBride, Bonnie, and Sanford Gordon, "Preliminary Description of CEC, A Computer Program for the Calculation of Chemical Equilibrium Compositions with Applications," NASA-Lewis Research Center, Cleveland, Ohio, 31 May 1968.

6. Komianos, S. A., G. D. Bleich and H. S. Pergament, "The AeroChem Nonequilibrium Streamline Program," AeroChem TN-103, AeroChem Research Laboratories, Inc., Princeton, N. J., May 1967.

7. Golden, J. O., and L. W. Spradley, "Description of a Digital Computer Code for Rocket Nozzle Sudden Freezing Analyses," LMSC/HREC A784526, Lockheed Missiles & Space Company, Huntsville, Ala., July 1967.

8. Robertson, S. J., "A Method for Calculating Flowfield Properties in Low Density Plumes," LMSC/HREC A784697, Lockheed Missiles & Space Company, Huntsville, Ala., October 1967.

9. Boynton, F. P., "Exhaust Plumes from Nozzles with Wall Boundary Layers," J. Spacecraft Roc., Vol. 5, October 1968, pp 1143 - 1147.

10. Smith, S. D., and A. W. Ratliff, "A Study of the Effect of a Boundary Layer along a Nozzle Wall on the Plume Flow Field," LMSC/HREC D149477, Lockheed Missiles & Space Company, Huntsville, Ala., 12 January 1970.

11. Ratliff, A. W., and J. W. Benefield, "Estimation of Accuracy of Rocket Exhaust Plume Flowfield Variables," LMSC/HREC A791939, Lockheed Missiles & Space Company, Huntsville, Ala., 2 July 1969.

12. Pieper, J. L., "ICRPG Liquid Propellant Thrust Chamber Performance Evaluation Manual," CPIA No. 178, Chemical Propulsion Information Agency, September 1968.

13. Audeh, B. J., "Effect of Freezing-Point Location on Specific Impulse Prediction," LMSC/HREC D149246, Lockheed Missiles & Space Company, Huntsville, Ala., October 1969.

Appendix A

SUPPLEMENTARY STUDY OF THE R-4D ENGINE USING N_2O_4/A-50 PROPELLANTS

Appendix A

A.1 INTRODUCTION

During study of the RCS motors for the Skylab configuration, experimental data from tests conducted at Manned Spacecraft Center (MSC) were used to help verify the analytical techniques and assumptions employed in the calculational scheme. Unfortunately, the test results were for an RCS engine (R-4D) using N_2O_4/A-50 propellants, whereas the Skylab configuration RCS engines utilize N_2O_4/MMH propellants. Nevertheless, it was deemed necessary to perform these correlations in order to determine the appropriate mixture ratio variation, since the engines are identical and only the propellants differ.

The experimental data indicated the presence of strong oxidizer-to-fuel-ratio (O/F) gradients and this fact was verified by injector mass flow and O/F distribution information received from the Marquardt Corporation. The experimental specific impulse (I_{sp}) was much lower than that computed by conventional means, also indicating the presence of O/F gradients, perhaps coupled with combustion inefficiency. Thus, a preliminary step in the study was to determine an appropriate O/F ratio gradient which would not only predict the I_{sp} more accurately, but would also correlate the experimental measurements of pitot pressure and heating rates across the plume near the exit plane of the nozzle.

A.2 DISCUSSION

A.2.1 Background

There were two basic measurements available, (1) pitot pressure and (2) stagnation point heating rate data from surveys made across the plume

near the exit plane and at several stations downstream of the exit. In addition, a measure of the engine efficiency was available by way of the I_{sp}. Initial effort directed toward determining the O/F ratio profile consisted of a two-pronged approach. Since the incoming or overall O/F ratio was known, it was used as a basic constraint on the system and the O/F profile at the nozzle throat was perturbed until the best fit of the pitot pressure data at the exit plane was obtained. Using the O/F ratio distribution determined in that manner, the I_{sp} was then examined to see if it was in line with the experimental value. The other approach (and the one which was ultimately selected due to its more fundamental nature) was based upon an analysis beginning at the injector face and proceeding throughout the engine. This approach accounts for mixing and burning between the various streams of differing O/F ratio in the combustion chamber as well as the two-dimensional effects in the transonic region. The supersonic expansion region was treated by the method of characteristics as in the preceeding approach.

A.2.2 Detailed Calculations

The O/F ratio distribution was determined from injector information and the assumption of constant mass flow per unit area. The centerline O/F value was fixed at the O/F ratio of the preigniter and the wall O/F value was determined from the overall O/F ratio, assuming a parabolic profile. These assumptions resulted in a distribution described by the following expression

$$\eta = 3.5 - 3.76\, r^2 ,$$

where η is the O/F ratio and r is the radial coordinate in inches at the injector.

Following the calculational scheme previously outlined, the engine nozzle and plume flowfield was computed. Correlations with experimental pitot pressures available are shown in Figs. A-1 through A-3. Figure A-4 shows the correlation for the stagnation point heating rate values.

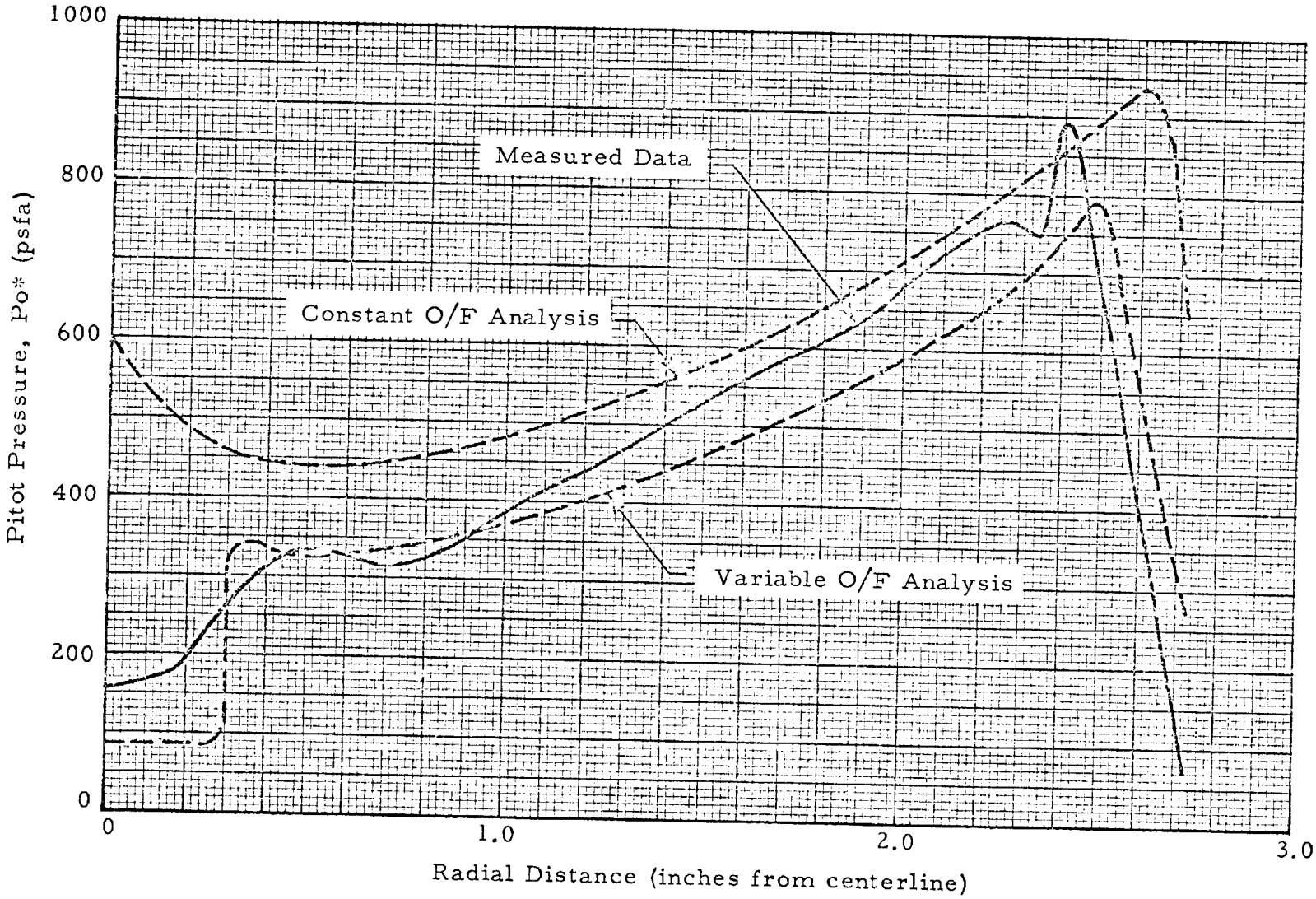

Fig. A-1 - Comparison of Measured and Calculated Pitot Pressures One-Half Inch Downstream of Exit Plane

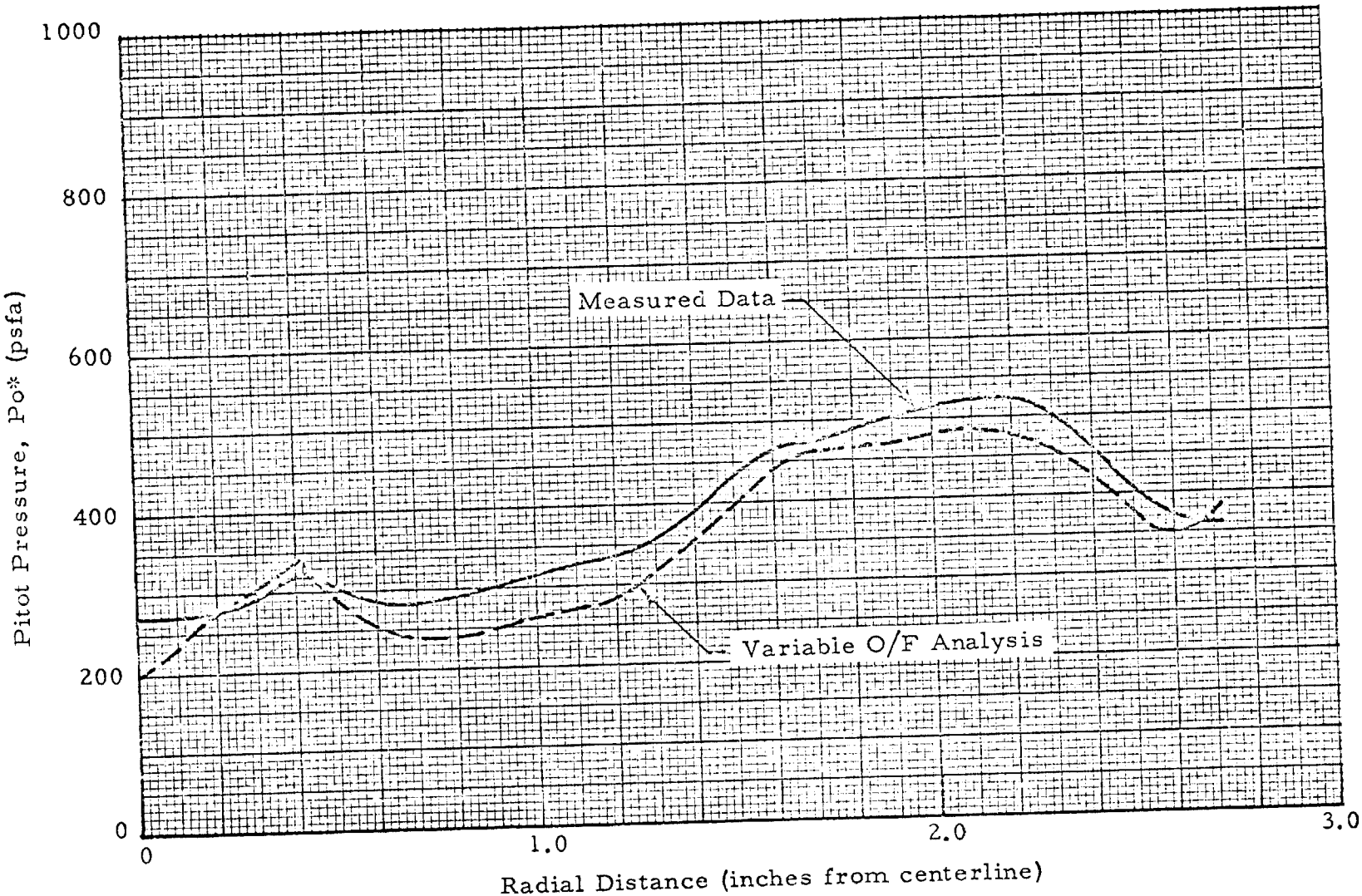

Fig. A-2 - Comparison of Measured and Calculated Pitot Pressures Three and One-Half Inches Downstream of Exit Plane

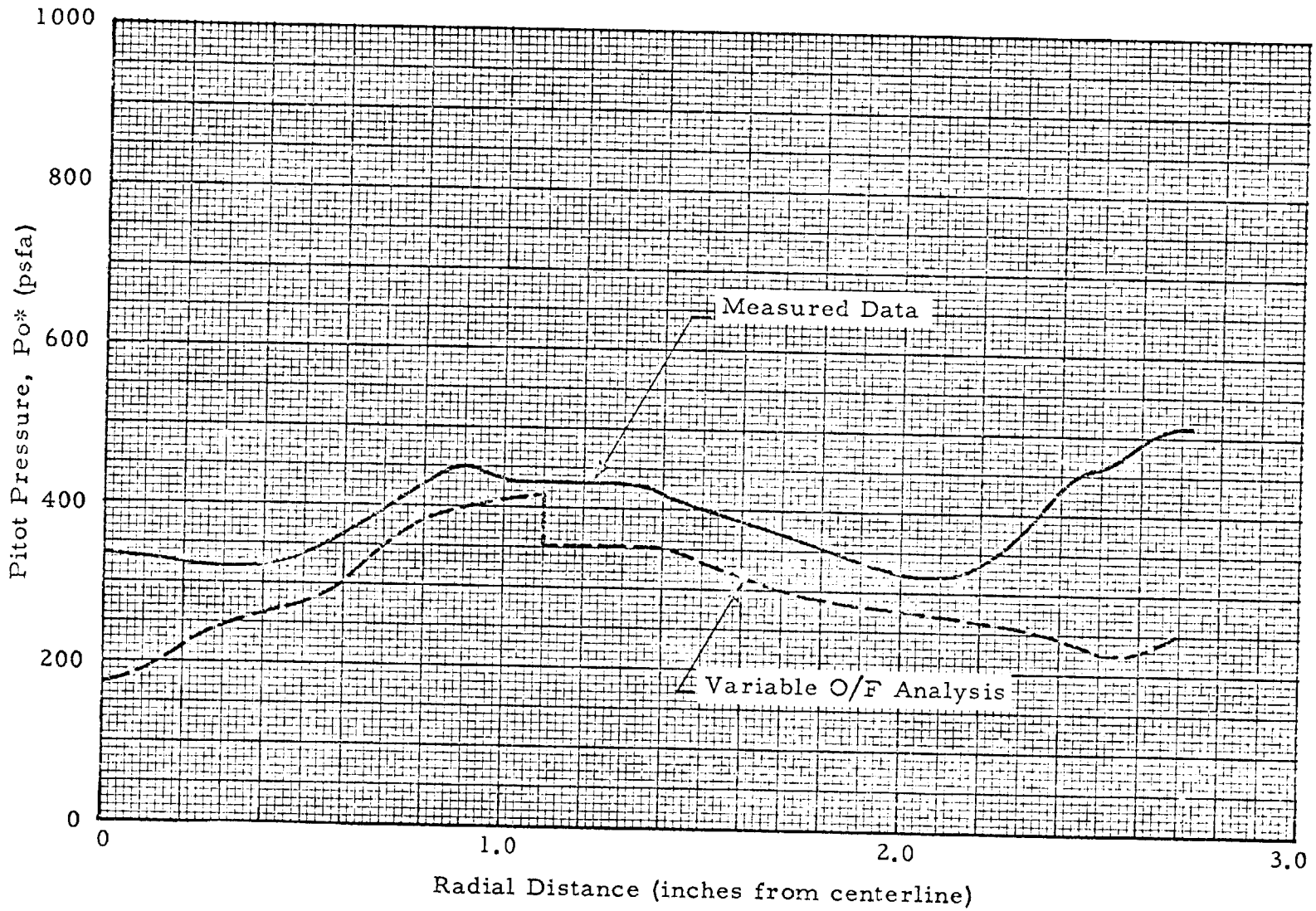

Fig. A-3 - Comparison of Measured and Calculated Pitot Pressures Six and One-Half Inches Downstream of Exit Plane

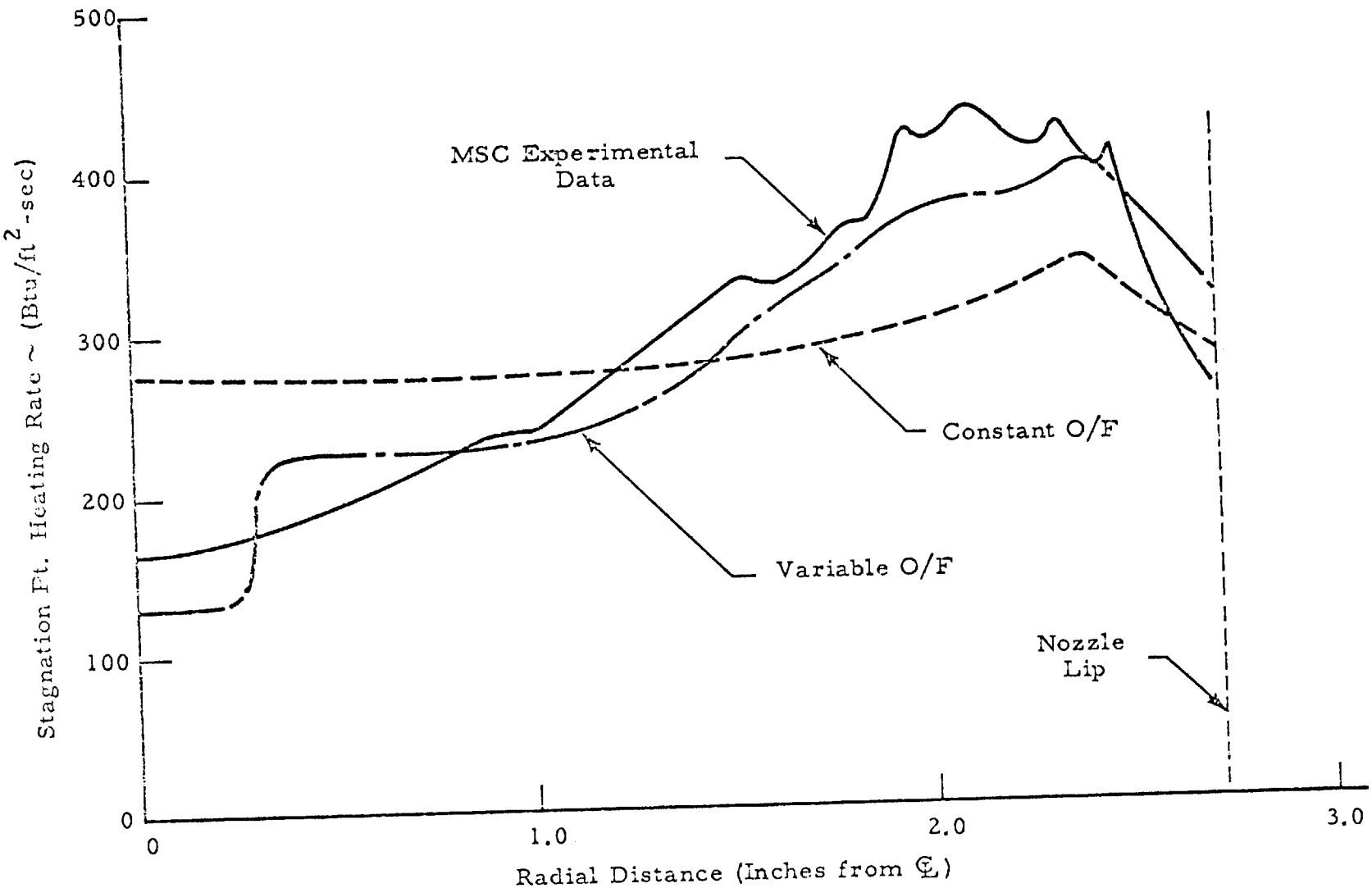

Fig. A-4 - Radial Heating Rate Variation 2.5 Inches From Exit Plane

In Fig. A-1 the measurements and calculations are for a plane 1/2-in. downstream of the nozzle exit. This figure shows the solution obtained from a non-distributed O/F ratio calculation fixed at a constant value of 2.0. As can be seen, the correlation, which assumes a constant O/F ratio is reasonable near the nozzle lip, but deviates quite badly near the centerline. Results from the distributed O/F ratio calculation also plotted on Fig. A-1 show significant improvement in the correlation, especially near the axis.

Some comment is in order concerning the relationship between the pitot pressure correlation near the centerline and the location of the shock wave generated by the reflex nozzle contour. The constant O/F ratio analysis does not even come close to predicting the proper shock location, whereas the distributed O/F ratio result correlates quite well. The measured pitot pressure data was noted to drop rapidly near the nozzle lip (the data were taken 1/2-in. downstream of the nozzle exit plane). The conclusion might be reached that this effect is due entirely to the nozzle lip expansion fan, but the analysis shows that this region is not greatly affected by the fan, but is actually altered greatly by the value of O/F ratio used at the wall. This effect is exemplified by comparing the pitot pressures near the nozzle lip. The constant O/F ratio value of 2.0, produces pitot pressures which are a factor of two higher than those predicted by the variable O/F ratio analysis along the streamline whose O/F ratio is 1.2. Here, of course, the variable O/F ratio result is much closer to the experimental value.

As previously mentioned, the measured I_{sp} was much lower than the constant O/F ratio prediction. The predicted I_{sp} using a constant O/F ratio analysis at the incoming mixture ratio value of 2.0 was 340 lb_f-sec/lb_m where the measured I_{sp} was 280 to 285 lb_f-sec/lb_m. The mixture ratio variation used in this analysis resulted in an I_{sp} prediction of about 300 lb_f-sec/lb_m, which means, of course, that in addition to the mixture ratio variation, there must also be some combustion inefficiency to account for the remainder of the performance degradation.

By arbitrarily reducing the propellant heats of formation, exactly the right I_{sp} can be produced; however, the objective of this study was not to predict performance but rather to describe the plume properties. Reducing propellant heats of formation had relatively little effect on correlating pitot pressure. The analytical curve tended to shift toward the centerline but its magnitude was not significantly altered. Since the plume property data will be used to design the vehicle, the data was generated without arbitrarily reducing the heats of formation in order to predict conservative design numbers.

Figures A-2 and A-3 present pitot pressure correlations at two other downstream stations and, as can be seen, the comparison is quite good, indicating that the analysis procedure utilized is applicable. In Fig. A-4 a comparison of the heating rates at a station $2\frac{1}{2}$-in downstream of the exit plane is shown. Without going into detail about the heating rate calculations note that the same procedure was used in calculating both the constant and the variable O/F ratio values so that any difference in the correlation is due strictly to the O/F gradient.

A.3 CONCLUSIONS

This auxiliary R-4D engine study was carried out, at least in part, to verify the analytical technique utilized for the study reported in the main body of this document. Comparison with measured pitot pressures, heating rates and performance parameters have shown that the procedure is quite adequate.

MSFC—RSA, Ala